Atmospheric response to the North Atlantic Ocean variability on seasonal to decadal time scales

Guillaume Gastineau *

Laboratoire d'Océanographie et du Climat: Expérimentations et Approches Numériques (LOCEAN),

IPSL/CNRS, Université Pierre et Marie Curie-Paris 6, Paris, France

Fabio D'Andrea

Laboratoire de Météorologie Dynamique (LMD),

IPSL/CNRS, Paris, France

Claude Frankignoul

Laboratoire d'Océanographie et du Climat: Expérimentations et Approches Numériques (LOCEAN),

IPSL/CNRS, Université Pierre et Marie Curie-Paris 6, Paris, France

Submitted to Climate Dynamics

* *Corresponding author address:* Dr. Guillaume Gastineau, LOCEAN/IPSL, Université Pierre et Marie Curie, 4 place Jussieu, BP100, 75252 Paris Cedex 05, France Tel.: +331-44-27-70-71 Fax: +331-44-27-38-05

E-mail: Guillaume.Gastineau@locean-ipsl.upmc.fr

ABSTRACT

The NCEP 20th century reanalyis and a 500-year control simulation with the IPSL-CM5 climate model are used to assess the influence of ocean-atmosphere coupling in the North Atlantic region at seasonal to decadal time scales. At the seasonal scale, the air-sea interaction patterns are similar in the model and observations. In both, a statistically significant summer sea surface temperature (SST) anomaly with a horseshoe shape leads an atmospheric signal that resembles the North Atlantic Oscillation (NAO) during the winter. The air-sea interactions in the model thus seem realistic, although the amplitude of the atmospheric signal is half that observed, and it is detected throughout the cold season, while it is significant only in late fall and early winter in the observations. In both model and observations, the North Atlantic horseshoe SST anomaly pattern is in part generated by the spring and summer internal atmospheric variability. In the model, the influence of the ocean dynamics can be assessed and is found to contribute to the SST anomaly, in particular at the decadal scale. Indeed, the North Atlantic SST anomalies that follow an intensification of the Atlantic meridional overturning circulation (AMOC) by about 9 years, or an intensification of a clockwise intergyre gyre in the Atlantic Ocean by 6 years, resemble the horseshoe pattern, and are also similar to the model Atlantic Multidecadal Oscillation (AMO). As the AMOC is shown to have a significant impact on the winter NAO, most strongly when it leads by 9 years, the decadal interactions in the model are consistent with the seasonal analysis. In the observations, there is also a strong correlation between the AMO and the SST horseshoe pattern that influences the NAO. The analogy with the coupled model suggests that the natural variability of the AMOC and the gyre circulation might influence the climate of the North Atlantic region at the decadal scale.

February 29th 2012

Keywords Air-sea interactions; North Atlantic; AMOC; Decadal variability

1. Introduction

Climate variability in the North Atlantic is dominated by the fluctuations of the jet stream position due to internal atmospheric variability, known as North Atlantic Oscillation (NAO). The NAO is mainly active during the winter season (Thompson and Wallace 1998), and is associated to the Arctic Oscillation, because of the interactions with the Pacific/North American pattern (Quadrelli and Wallace 2004). The NAO is the dominant mode of climate variability over the North Atlantic region and it modulates a large fraction of the variance of precipitation and temperature over Europe and North America. The NAO also generates the sea surface temperature (SST) anomaly tripole, which has a pole off Cape Hatteras, and two poles with an opposite polarity in the subpolar region and the eastern subtropical Atlantic. The tripole is driven by turbulent heat flux anomalies and, to a lesser extent, by the anomalous Ekman advection associated with the NAO (Cayan 1992; Deser et al. 2009).

On short time scales, the temporal evolution of the NAO is consistent with a first-order Markov process with an e-folding timescale of about 10 days (Feldstein 2000). The ocean mixed layer integrates the atmospheric variability into a red noise like signal, enhancing the low frequency variability (Frankignoul and Hasselmann 1977). Several studies point to a weak feedback of the ocean onto the NAO that may slightly increase the power density spectrum of the NAO at the interannual to decadal frequency band. In observations, Czaja and Frankignoul (1999, 2002) showed that a tripolar horseshoe-like SST anomaly in late summer has a significant influence on the winter NAO. The North Atlantic horseshoe (NAH) SST anomaly, which is somewhat different from the tripole generated by the NAO, was suggested to be itself triggered by the atmospheric variability during the summer season. However, the possible role of the ocean dynamics has not been investigated. A similar influence of the ocean was also established using atmospheric GCM experiments. For instance, Watanabe and Kimoto (2000) and Peng et al. (2003) found that the SST anomaly tripole also has an influence on the NAO mainly during winter, acting as a positive feedback.

The SST in the Atlantic Ocean also displays in both the historical record (Kushnir 1994) or paleoproxies (Mann et al. 1998; Gray et al. 2004) a marked multidecadal variability with a 65-80 yr period, called the Atlantic Multidecadal Oscillation (AMO). In its positive phase, the AMO primarily reflects a warming of much of the North Atlantic with maximum SST anomaly in the subpolar region, and a weak cooling in the South Atlantic. It is considered to be largely driven by the variability of the Atlantic meridional overturning circulation (AMOC), and climate model simulations show that a stronger AMOC leads to an increased oceanic northward heat transport and, after some delay, a SST warming in the North Atlantic (e.g. Delworth and Greatbatch 2000; Knight et al. 2005). However, the AMO is also affected by global warming (Trenberth and Shea 2006) and by other climatic modes of variability such as El Niño Southern Oscillation (ENSO), so its pattern may not solely reflect the AMOC influence (Dong et al. 2006; Guan and Nigam 2009; Compo and Sardeshmukh 2010; Marini and Frankignoul 2012). The climatic impact of the AMO has been assessed with atmospheric GCM runs with prescribed SST anomalies, which primarily suggests that the tropical warming in a positive AMO phase changes the atmospheric circulation during summer similarly to a Gill-like response to the diabatic latent heating in the Caribbean Basin (Sutton and Hodson 2005, 2007; Hodson et al. 2010). An impact of the AMO onto the summer NAO was suggested by Folland et al. (2009), but the mechanism for this AMO influence remains to be found. So far, no robust impact onto the winter NAO was reported.

As the climatic impact of the ocean dynamics and in particular the AMOC cannot be established from sparse observations, climate models have to be used. Conceptual models (Marshall et al. 2001) or more intermediate complexity models (Eden and Greatbatch 2003) suggest that the ocean dynamics could influence the NAO by modulating the North Atlantic SST through changes in the heat transport by the AMOC. In 6 climate models, Gastineau and Frankignoul (2011) found that an AMOC intensification leads to a weak negative NAO phase during winter, after a delay of a few years. This NAO signal was interpreted as the modulation of the North Atlantic storm track by the SST changes that followed an AMOC increase. These SST anomalies were similar to the model AMOs. If the decadal AMOC and AMO variations indeed influence the NAO, the interaction should be seen in the observations at the seasonal scale, since the atmospheric response time is a few months at most. However, as the signal-to-noise ratio may be low in the observations due to data limitations and uncertainties, it is of interest to first consider a coupled model where a much larger sample is available and, in addition, the AMOC is known.

The horizontal gyre circulation has also been shown to influence the North Atlantic SST anomalies in conceptual models Marshall et al. (2001); Czaja and Marshall (2001); D'Andrea et al. (2005), or in coupled models Bellucci et al. (2008); Schneider and Fan (2012). In these studies the NAO produces an intergyre gyre, resembling the subtropical gyre, but extending farther north, after a delay of several years. The intergyre gyre then modifies the SST anomalies in the North Atlantic through the heat advection, and enhances the SST and NAO decadal variability in some cases.

The main purpose of this paper is to investigate the interactions between the North Atlantic Ocean and the atmosphere in IPSL-CM5, the version 5 of the Institut Pierre Simon Laplace (IPSL) climate model, with a focus on the oceanic influence on the atmosphere. The model validity is first established by comparison with observations. As the model is found to reproduce successfully much of the observed features of the North Atlantic air-sea interactions at the seasonal scale, it is then used to explore the links between the air-sea interactions at the seasonal and decadal scales. A main result of this paper is that the SST anomalies that influence the NAO at the seasonal scale are strongly influenced in the model by the low-frequency variability of the AMOC and to a lesser extend by the intergyre gyre. The atmospheric impacts of the AMOC occur via a modulation of the SST anomalies that resemble the NAH SST pattern found at the seasonal scale.

The model and data are presented in the next section. The ocean-atmosphere relationships during the seasonal cycle are evaluated in section 3. Section 4 investigates the influence of the ocean dynamics, and the last section is devoted to discussion and conclusions.

2. Model and data

a. Observations

To investigate the air-sea interactions at both seasonal and decadal scales, we use the longest available reanalysis, the 20th century NCEP reanalysis during the period 1901-2005 (Compo et al. 2011). The 20th century NCEP reanalysis assimilates only surface pressure reports, using an ensemble von Kalman filter assimilation method. It uses a recent version of the NCEP-GFS model and is forced with the HadISST sea-ice and SST (Rayner et al. 2003). The North Atlantic is a well sampled region and the reanalysis provides a state of the art estimation for the climate variability of the 20th century, with well quantified uncertainties. Here, we only use the 500-hPa geopotential height anomaly data. The 500-hPa geopotential height and assimilated sea-level pressure are expected to be strongly linked, because of the equivalent barotropic character of the main patterns of extratropical atmospheric variability (Peng and Whitaker 1999). The 500-hPa geopotential height from the reanalysis was also previously validated using independent observation from the 20th century (Stickler et al. 2009; Compo et al. 2011). Lacking a better model, a third order trend is removed from the geopotential height prior to analysis to eliminate the effect of global warming.

The HadISST dataset is used for the SST anomalies. The SST is strongly influenced by the warming trend due to increasing greenhouse gas concentrations during the 20th century. This influence needs to be carefully filtered when estimating the natural decadal or multidecadal variability. Previous studies have removed a linear (e.g. Sutton and Hodson 2005) or a quadratic (Enfield and Cid-Serrano 2010) trend while Trenberth and Shea (2006) removed the global mean of the SST fields in order to retrieve the low frequency variability. In this study, we use the data of Marini and Frankignoul (2012), where linear inverse modeling (LIM, e.g. Penland and Matrosova 2006) was used to remove the global warming signal in the HadISST data of the 1901-2005 period. Indeed, in a 20th century simulation of IPSL-CM5, the LIM filter provided an AMO estimation that had a larger correlation with the AMOC than the secular trend removal by other methods (see Tab. 2 in Marini and Frankignoul 2012). We call these data HadISST-LIM. The HadISST-LIM data are available between 0°N-60°N, for 4 seasons JFM, AMJ, JAS and OND. We reconstructed monthly outputs by linear temporal interpolation.

b. *Model*

IPSL-CM5 is the version 5 of the IPSL climate model involved in the phase 5 of the Coupled Model Intercomparison Project (CMIP5). As described in Dufresne et al. (2012), the model uses the atmosphere model LMDZ5A (Laboratoire Météorologie Dynamique GCM version 5, where Z stands for ”zoom”, while A indicates standard physical parametrizations; see Hourdin et al. 2012a for details), the ocean model NEMO

(Nucleus for European Modeling of the Ocean, Madec et al. 1998) and the ORCHIDEE (Organizing Carbon and Hydrology in Dynamic Ecosystems) land surface model (Krinner et al. 2005), coupled with the OASIS3 module (Ocean Atmosphere Sea Ice Soil version 3, Valcke 2006). The version of IPSL-CM5 used is IPSL-CM5A-LR, where LR stands for low resolution and A indicates that atmospheric physical parameterizations are minimally modified compared to the previous version of the IPSL model. This simulation uses a low atmospheric resolution of $3.75° \times 1.9°$ and 39 vertical levels, and an oceanic resolution of about 2° and 31 levels, with a finer oceanic grid of 0.5° at the equator. The main difference with IPSL-CM4 is the increased latitudinal and vertical atmospheric resolution, which improves the position of the jet streams and the storm tracks, although they are still shifted a few degrees equatorward (Guemas and Codron 2011; Hourdin et al. 2012a). The stratosphere is also better resolved with 15 levels in the stratosphere, up to 1hPa (Maury et al. 2012). In IPSL-CM5, the Gulf Stream is too weak, as in most low resolution models, and too equatorward. As shown below, the AMOC is of the order of 10 Sv, which is low compared to observations (Cunningham et al. 2007), other climate models (Medhaug and Furevik 2011), or oceanic reanalyses (Munoz et al. 2011), that show an AMOC within the range of 12-30 Sv. The weak AMOC is related to the large extension of the winter sea-ice due to a cold bias in midlatitudes (Dufresne et al. 2012), as in the previous version of the model (Msadek and Frankignoul 2009). This prevents the oceanic convection from happening in the Labrador Sea, so that the main convection site is located South of Iceland. Here, we use a preindustrial control simulation of 500 years, after several hundred years of spin-up. Although the simulation is relatively stable, we removed a second order trend from all model outputs prior to analysis.

The first two empirical orthogonal functions (EOFs) of the winter 500-hPa geopotential height over the North Atlantic (Fig. 1) show the main patterns of atmospheric variability in IPSL-CM5. Here and in the following, EOFs are displayed as regression maps onto the corresponding normalized Principal Component (PC), so that the EOFs show the typical amplitude of the fluctuations. The first EOF is the NAO (Hurrell et al. 2003), shown here in its negative phase. Its pattern is realistic, although shifted a few degrees north compared to observations. The second EOF is the East Atlantic Pattern (EAP), with a pattern similar to observations. Rotated EOFs (not shown) provide a sightly better estimation of the NAO and shift the geopotential anomalies southward. However, for simplicity, we only show results without rotation. The overall atmospheric variability is broadly similar to that of IPSL-CM4 (Msadek and Frankignoul 2009).

3. SST influence onto atmosphere during the seasonal cycle

a. *Method*

The main patterns of covariability between the ocean and the atmosphere are studied with a Maximum Covariance Analysis (MCA), which performs a singular value decomposition of the covariance matrix between atmospheric and oceanic anomaly fields. The lag MCA has been extensively used to distinguish between cause and effect in air-sea interactions (e.g. Czaja and Frankignoul 2002; Frankignoul et al. 2011). The reader is referred to Bretherton et al. (1992), for a more complete description of the MCA. Here, the two fields used are the 500-hPa geopotential height (Z500) in the North Atlantic sector (20°N-80°N, 100°W-20°E) and the underlying SST (100°W-20°E and 0°-70°N for the model and 0°-60°N for HadISST-LIM). The regions where the climatological sea-ice coverage exceeds 50% are excluded from the analysis. Note that the results below are not sensitive to the precise limits of the domain and the sea-ice threshold.

Running three-month averages are computed for the SST and Z500 anomalies. As the intrinsic atmospheric persistence is less than 1 month and that of the ocean much larger, a significant lagged relation between the ocean and the atmosphere when the ocean leads by more than 1 month indicates an oceanic (or other boundary forcing) influence onto the atmosphere, if monthly fields are used. Conversely, when the atmosphere leads, the ocean influence onto the atmosphere is masked by the much larger atmospheric influence onto the ocean. As three-month averages are used to define each calendar month, only the lags larger than 3 months can be considered to reflect solely the oceanic influence in IPSL-CM5, lower lags being contaminated by the atmospheric influence onto the ocean. For HadISST-LIM, the lags should be larger than 3 to 5 months, depending on the calendar month, to fully reflect the oceanic influence, because of the linear temporal interpolation used.

The additional atmospheric persistence due to ENSO complicates these relationships, as lagged relations between ocean and atmosphere might also result from the remote ENSO teleconnection onto the North Atlantic region (see Appendix). Frankignoul and Kestenare (2002) have shown that the ENSO influence on the atmospheric response to extratropical SST could be largely removed by substituting the anomalies of Z500 and SST, referred to as $\mathbf{Z}(t)$ and $\mathbf{T}(t)$, by $\mathbf{Z}(t) - \mathbf{a}N_1(t) - \mathbf{b}N_2(t)$ and $\mathbf{T}(t) - \mathbf{c}N_1(t) - \mathbf{d}N_2(t)$, where $N_1(t)$ and $N_2(t)$ are the first two PCs of the SST in the equatorial Pacific Ocean (12.5°S-12.5°N, 100°E-80°W), and $\mathbf{a}$, $\mathbf{b}$, $\mathbf{c}$ and $\mathbf{d}$ are regression coefficients determined by least square fits of the SST onto $N_1(t)$ and $N_2(t)$, for each grid point in the North Atlantic. Three-month running averages are used to compute the PCs of the SST in the Equatorial Pacific. Note that non-linear effects are neglected, so that the ENSO signal may not be completely removed (OrtizBeviá et al. 2010). Furthermore, the ENSO signal may take 1 or 2 month to influence the mid-latitude variability, but since three-month means are used, we will consider the ENSO teleconnection over North Atlantic as instantaneous.

The MCA isolates K pairs of spatial patterns and their associated time series :

$$\mathbf{Z}(t) = \sum_{k=1}^{K} \mathbf{u}_k a_k(t) \tag{1}$$

$$\mathbf{T}(t-\tau) = \sum_{i=1}^{K} \mathbf{v}_i b_i(t-\tau) \tag{2}$$

where τ is the time lag, positive when the ocean leads the atmosphere. $\mathbf{u}_k$ and $\mathbf{v}_k$ are the left and right singular vectors, with $\mathbf{u}_k.\mathbf{u}_l = \delta_{kl}$ and $\mathbf{v}_i.\mathbf{v}_j = \delta_{ij}$. The covariance between a_k and b_i, the times series associated with the left and right singular vectors, respectively, is maximum for $k = i$, and the time series are orthogonal to one another between the two fields, e.g. $cov(a_k, b_i) = \sigma_k \delta_{ki}$. Here, σ_k is the covariance explained by the pair of left and right singular vectors, $\mathbf{u}_k$ and $\mathbf{v}_k$. Note that in the MCA, the Z500 and SST are weighted by the square root of the cosine of the latitude, for area weighting.

Note that the singular vectors $\mathbf{u}_k$ and $\mathbf{v}_k$ are not linearly related, so that heterogeneous and homogeneous map pairs are preferably shown to ease the interpretation of the MCA modes (Czaja and Frankignoul 2002). The homogeneous maps for the ocean and heterogeneous maps for the atmosphere, defined as the projections of the Z500 and SST onto $b_k(t-\tau)$, are shown to study the influence of the ocean onto the atmosphere. When studying the oceanic response to the atmosphere, it is preferable to show the heterogeneous SST and homogeneous Z500, which are the projections of both fields onto $a_k(t)$.

Careful statistical testing is required to identify whether the modes of variability are meaningful. For each lag, the statistical significance of the squared covariance and correlation between the time series $a_k(t)$

and $b_k(t-\tau)$ is assessed with a Monte Carlo approach, by comparing the squared covariance and correlation to that of a randomly scrambled ensemble. We randomly permute the Z500 time series by blocks of 3 years to reduce the influence of serial autocorrelation, and perform an MCA. We repeat this analysis 100 times. The estimated statistical significance level is the percentage of randomized squared covariance (correlation) that exceeds the squared covariance (correlation) being tested. It is an estimate of the risk of rejecting the null hypothesis (there is no relation between the Z500 and the SST) when it is true.

b. *Results*

The interactions between the SST and the atmospheric variability are expected to be seasonally dependent. On the one hand, the atmospheric dynamic differs during the seasonal cycle, with different interactions between the mean atmospheric flow and eddy fields (Peng and Whitaker 1999; Peng et al. 2003). On the other hand, the oceanic influence onto the atmosphere is expected to be most persistent between late fall and spring when the oceanic mixing layer is deepest, and when SST reemergence is expected to occur (Cassou et al. 2007). The squared covariance of the first MCA mode is shown in Fig. 2 as a function of season and lag. Here and in the following, we focus on the first MCA mode, which is the only one that shows a significant atmospheric response to the ocean. Its squared covariance fraction is typically between 50% and 80% (40% and 70%) for observations (IPSL-CM5), while it is between 10% and 30% (10% and 40%) for the second mode, depending on the season.

In observations (Fig. 2, right panel), the squared covariance is largest and most significant for the negative lags (lag < 0), with a maximum when the atmosphere leads the ocean by two months, in winter season (Z500 in JFM). It reflects the stochastic forcing of the ocean by the atmosphere, which is strongest during winter (Frankignoul and Hasselmann 1977; Kushnir 1994). When the ocean and atmosphere are in phase, or when the ocean leads by 1 to 2 months, the squared covariance is still large and significant and it also reflects the atmospheric forcing of the ocean. When the ocean leads by more than 2 month (lag ≥ 3), the squared covariance is much lower and less significant. However a weak maximum which is 10% to 5% significant is found for Z500 in NDJ, when SST leads by 5 to 8 months. It shows that the ocean has a significant impact onto the atmosphere in early winter, as found by (Czaja and Frankignoul 1999, 2002).

The same analysis in the IPSL-CM5 model (Fig. 2, left panel) shows comparable results, even if the squared covariances are 50% weaker and more significant. The strongest squared covariance is found when the atmosphere leads by two months for Z500 in JFM and FMA. When SST leads by more than 2 month (lag ≥ 3), IPSL-CM5 also shows a local maximum between lag 5 and 9 months, which is 5% significant for Z500 in DJF, JFM and FMA. Note that some significant squared covariances also appear when ocean leads by up to 10 month for the JAS Z500, but in the following, we will only focus on the cold season atmosphere.

The generally higher significance in the model simulation may come from the longer time series used for the model simulation (500 yr) compared to observations (105 yr), as well as the uncertainties in the latter. The seasonality of the atmospheric response to the ocean is similar to that found in atmospheric GCM experiments forced by SST anomalies similar to the NAO-related tripole, which usually provide a strongest atmospheric signal in late winter (Peng et al. 2002; Deser et al. 2007; Cassou et al. 2007). The fact that the atmospheric response is only significant during late fall–early winter in the 20th century NCEP reanalysis may be related to a larger signal-to-noise ratio, as the atmospheric variability is weaker during this season than later in winter.

Figure 3 presents the homogeneous and heterogeneous maps for Z500 and SST in IPSL-CM5, focusing on the winter atmospheric Z500 response (JFM) and lags ranging from -1 to 7 months, the lag being positive when the ocean leads. When the atmosphere leads the ocean (lag -1), the first MCA mode shows the NAO in its negative phase, and its influence onto the underlying SST. The NAO causes the apparition of the North Atlantic SST tripole, with SST anomalies of one polarity in the subpolar region and the eastern subtropical Atlantic, and the opposite polarity off the east coast of North America. When the ocean and atmosphere are in phase, the atmospheric influence onto the ocean dominates and the MCA results are similar to those when the atmosphere leads. The atmospheric forcing influence still contaminates the results for lag 1 and 2 as three-month means are used for each season. Note that the second MCA mode (not shown), shows the influence of the EAP (EOF2 of Z500 in Fig. 1) onto the SST, anticyclonic Z500 anomalies over the North Atlantic Basin being associated with a tripole-like SST pattern shifted northward with large SST anomalies located between 45°N and 50°N, off the coast of Newfoundland.

When the ocean leads the atmosphere by 3 months or more, the first MCA mode represents the oceanic influence onto the atmosphere. The main pattern of co-variability describes a somewhat different SST anomaly, which leads a NAO-like Z500 signal. The SST pattern is characterized by a crescent shape warming with maximum amplitude in the subpolar basin, surrounding a cooling of the western Atlantic between Cape Hatteras and Newfoundland, thus forming a horseshoe pattern. The corresponding Z500 anomalies form a dipole, with positive Z500 anomalies over the subpolar basin, centered South of Iceland, weaker negative anomalies from Southern United States to the Iberian Peninsula, and a zero line going from Newfoundland to the British Island: the overall pattern resembling a negative NAO, slightly shifted southwards. In terms of amplitude, the ratio of the maximum Z500 anomalies over the maximum SST anomalies is of the order of 10 m K^{-1}. Results for DJF or FMA are similar to those obtained for JFM (not shown).

To compare the model with observations, the same analysis using the NCEP 20th century 500-hPa geopotential height and the HadISST-LIM SST is shown in Fig. 4. Here, we repeated the analysis of Czaja and Frankignoul (2002) but using longer reanalysis dataset to better take into account the likely SST modulation by the AMOC, albeit with a loss of accuracy since observations are sparser during the first half of the record. Note that the color scale in Fig. 4 is modified compared to Fig. 3, to better illustrate the SST patterns. Here, we show the atmosphere during early winter (NDJ), as this season corresponds to the most significant oceanic influence (see Fig. 2). Note that in Fig. 4, only the lags larger than 4 can truly show an impact of the SST, as three-month running means in HadISST-LIM are reconstructed from a linear temporal interpolation, and NDJ illustrated here is reconstructed from OND and JFM. The similarity between the spatial patterns of the SST and Z500 in the model and observations is remarkable in both lead and lag conditions. Nevertheless, when the atmosphere leads, the SST tripole has a more extended subtropical Atlantic pole in the observations. When the ocean leads, the observational results reveal a subpolar SST warming that is shifted westward compared to the model, and a stronger and southward shifted subtropical SST warming with another maximum off the coast of Senegal and Morocco. The differences are consistent with a systematic underestimation in IPSL-CM5 of the SST variability in the eastern tropical North Atlantic, off the coast of Africa. The observed SST variability in this region is enhanced by a wind-driven positive heat flux feedback in summer (Czaja et al. 2002). IPSL-CM5 may underestimate the amplitude of this mechanism, which might be linked to the poor representation of the wind in response to convection over the African continent (Hourdin et al. 2012b). In terms of amplitude, the intensity of the observed response is of the order of 25 m K^{-1}, therefore the model underestimates the atmospheric response. In both IPSL-CM5 and observations, as the NAH pattern broadly resembles the SST anomaly tripole, the SST anomalies tend to reinforce the atmospheric anomalies that contributed to their generation, thus acting as a positive feedback. In the following, NAH designates summer and fall SST anomalies leading the NAO, while SST-tripole designates the NAO simultaneous SST anomalies, even if both spatial pattern are simimar.

The origin of the SST NAH pattern has not been fully investigated yet, although Czaja and Frankignoul (2002) showed that the intrinsic atmospheric variability generates SST anomalies similar to the NAH in summer. However, the oceanic variability may also exert an influence onto the SST anomalies, as discussed below.

4. Origin of the oceanic influence

a. Atlantic Meridional Overturning Circulation

The AMOC could potentially influence the SST anomalies responsible for the atmospheric response, and thus have an influence onto the atmosphere at decadal and multidecadal time scales. The mean AMOC of IPSL-CM5 is shown in Fig. 5 (upper-left panel). The maximum value of the AMOC is of the order of 10 Sv, which is linked to some well known deficiencies in the model wind speed and a cold bias in midlatitudes (see section 2.b). The AMOC has been shown to have an oscillating eigenmode in an adjoint version of the ocean-only model used in IPSL-CM5 (Sevellec and Fedorov 2012). Escudier et al. (2012) showed that in this IPSL-CM5 simulation, the oceanic variability has a significant 20 year cycle linked to propagation of temperature and salinity anomaly within the subpolar gyre, sharing some similarities with the eigenmode of Sevellec and Fedorov (2012), but modified and amplified by ocean-sea ice-atmosphere interactions in the Nordic Seas.

The first EOF of the AMOC in IPSL-CM5 is shown in Fig. 5 (upper-right panel). It represents in this polarity an intensification and deepening of the mean AMOC, with maximum amplitude between 30°N and 60°N. A spectrum of the PC1 of the AMOC (not shown) clearly shows a few significant peaks of variability between 20 and 30 yr.

In both model and observations, the AMO is defined by the mean North Atlantic SST between 10°N and 60°N filtered with a 10 yr cut-off period to only retain the low frequency variability (Fig. 5, lower panels). The AMO patterns are similar, with a subpolar positive SST anomaly and a comma-shaped positive anomaly following the eastern subtropical gyre. However, the model AMO indicates a stronger warming in the subpolar North Atlantic, while in the subtropics the model SST anomaly is shifted northward compared to observations. The AMO in IPSL-CM5 has weak negative SST anomalies at the sea-ice edge in the Nordic seas and between Iceland and Greenland, which reflect the role of the East Greenland Current in driving the AMOC and the AMO (Escudier et al. 2012). The cooling of the western subtropical Atlantic is also weaker than observed.

The SST signal following an AMOC intensification in the model is illustrated by a regression of the SST onto the normalized first PC of the AMOC as a function of time lag (Fig. 6), for summer (JAS) and fall (OND). Very similar anomalies are obtained in the other seasons. Here and in the following, the significance level for each grid point is established by Monte Carlo analysis, with 100 random permutations of the SST by blocks of 3 years. In phase, the AMOC intensification is related to a cold subpolar basin and a warm subtropical North Atlantic, in particular off the coast of North America. The subpolar basin south of Iceland, where deep convection occurs in the model, is cold in part due to the mixing of the surface and deep waters which took place a few years before the AMOC intensification. As shown in Eden and Willebrand (2001); Deshayes and Frankignoul (2008); Gastineau and Frankignoul (2011), most models show a negative AMOC anomaly in the subpolar regions and a positive one in the subtropics as a fast response to a positive NAO, consistent with the anomalous Ekman pumping and the deep return flow driven by the NAO surface wind stress. The NAO also causes the apparition of the North Atlantic SST tripole, through the modification of the surface heat fluxes (see Figs. 3 and 4). After an AMOC intensification, the poleward heat transport increases and a strong warming develops in the subpolar basin. The positive SST anomalies are first located in the North Atlantic current region, then propagate into the subpolar region by lag 3, expanding and intensifying until they reach a maximum at 9 yr lag. At the same time, the warming spreads in the subtropical gyre while cooling occurs in the Gulf Stream region, so that the SST anomaly forms a comma-shaped pattern in the North Atlantic. The similarity between the AMOC-induced SST and the AMO in the model is striking (compare lower-left panel of Fig. 5 and the lower panels of Fig. 6), as in most climate models (Knight et al. 2005; Msadek and Frankignoul 2009), even if the lag between the AMOC and AMO is model dependent (Marini and Frankignoul 2012).

The AMOC-induced SSTs also have strong similarities with the NAH pattern found in the MCA (compare with Fig. 3, lag 6 or 7). In Fig. 7, we computed the spatial correlation between the SSTs regressed onto AMOC-PC1 at different lags in years and the SST NAH pattern, which is given by the homogeneous SST map in Fig. 3 when the SST leads the JFM negative NAO by 3 months (SST in OND) and 6 months (SST in JAS). The significance of the spatial correlations are based on the 5% and 10% strongest spatial correlations obtained in an ensemble of 200 randomly scrambled AMOC time series, using blocks of 3 years to account for autocorrelation.

In summer (JAS, Fig. 7, upper-left panel), the SST patterns have a broad and significant positive spatial correlation, which reaches its maximum 9 yr after the AMOC in summer (JAS), while a weaker negative correlation is found in phase. The negative in phase correlation is due to the NAO simultaneously influencing the SST and the AMOC, as a negative phase of the NAO causes tripolar SST anomalies that have similarities with the NAH, while it weakly decreases the AMOC (Gastineau and Frankignoul 2011). On the other hand, as shown in Fig. 6, the SST is progressively modulated by the currents associated with an AMOC intensification until the SST anomaly reaches the horseshoe-shape at lag 6 to 13 years that can optimally force an atmospheric signal. In fall (OND, Fig. 7, lower-left panel), a larger negative correlation is obtained in phase, as the NAO is more active during this season. A weakly significant positive correlation is still obtained when the AMOC leads by 11 yr, which indicates a weaker but statistically significant AMOC influence onto the NAH.

The cold-season atmospheric response to the AMOC has been discussed in Gastineau and Frankignoul (2011), who showed that it was most significant when the AMOC leads by 9 yr in IPSL-CM5, with a negative phase of the NAO following an AMOC intensification. The pathways of the winter atmospheric response to the AMOC in IPSL-CM5 are presented for lag 9 in Fig. 8, with the regressions onto the normalized AMOC-PC1 of the winter (JFM) SST, heat flux, 850-hPa maximum Eady growth rate and 500-hPa transient eddy activity. Note that the storm track intensity is calculated from daily outputs.

The SST anomalies in the North Atlantic modify the heat exchanges between the ocean and the atmosphere, the atmosphere acting as a negative feedback that damps the SST anomalies as in Frankignoul and Kestenare (2002) and Park et al. (2005). This increases the upward heat flux in the southern subpolar basin, where the SST anomalies are the largest, and decreases it further north. In the Gulf Stream/North Atlantic Current region where the climatological heat flux is maximum, the heat flux decreases to the north and increases to the south, thus shifting the ocean forcing southward. These changes contribute to the decrease of the storm track intensity and shift the storm track southward, as shown by the maximum Eady growth rate at 850-hPa (Fig. 8, lower-left panel) and the 500-hPa geopotential height standard deviation (Fig. 8, lower-right panel), leading to a negative NAO phase. We suspect that it is the reduction (amplification) of meridional SST gradient in southern (northern) subpolar region, together with the southward shift in the Gulf Stream/North Atlantic Current region, which causes the overall decrease of the storm track and the negative NAO response. The signal is similar in IPSL-CM4, which was illustrated in Gastineau and Frankignoul (2011), but the atmospheric response is stronger and more significant in IPSL-CM5.

b. Atlantic Gyre Circulation

The mean gyre circulation of IPSL-CM5 shows a clockwise subtropical gyre centered at 30°N, and a counterclockwise subpolar gyre centered at 55°N (not shown). The circulation within the subtropical gyre reaches 35 Sv, which is comparable to observational estimates (Schott et al. 1988). The first two EOFs of the barotropic streamfunction are shown in Fig. 9, positive values indicating clockwise circulation. The first EOF indicates a modulation of the gyre circulation magnitude, that represents 26% of the variance. Escudier et al. (2012) showed that the modulation of the gyre intensity is influenced by the 20-yr oceanic cycle, which also influences the AMOC. The modulation of the gyre intensity is therefore difficult to distinguish from the AMOC variability, as causes and effects are not easily separable, and it is not considered further. The second EOF (21%) shows a large clockwise gyre shifted northward compared the mean subtropical gyre, often called the intergyre gyre, that extends northward up to the Labrador Sea in the eastern subpolar region. It is driven by the NAO, with a high simultaneous correlation between yearly values ($r = 0.65$), a positive NAO causing an IGG intensification.

The influence of the intergyre gyre on the SST is calculated by regressing the SST onto PC2 time series, hereafter called IGG (intergyre gyre) index (Fig. 10). The simultaneous regression map reflects that the IGG is forced by the NAO, which also generates the SST tripole, with a polarity opposite to that shown in Fig. 3. After a delay of about 3 years, warm SST anomalies appear in subpolar basin, together with a tongue of warm SSTs from Spain to the center of the Atlantic Ocean. The strongest SST anomalies appears after 6 years and then slowly decrease. Figure 10 shows that the SST anomalies driven by, or at least following an IGG intensification also share some similarities with the NAH, even if they are weaker than the SST anomalies associated with the AMOC.

The spatial correlation between the SST regression onto the IGG and the NAH is illustrated in Fig.7. As noted before, the simultaneous correlation reflects that a positive NAO causes a NAH-like SST, with a negative polarity using our conventions. When the IGG leads, it primarily reflects its modulation of the SST, with a pattern that has a significant maximum spatial correlation with the NAH after 4 to 7 years, during JAS and OND. An intensification of the IGG is thus followed by the NAH, which drives a negative phase of the NAO. In IPSL-CM5, the IGG thus exerts a negative feedback onto the NAO variability, as found in Czaja et al. (2002); Bellucci et al. (2008).

c. Atmospheric stochastic variability

The atmosphere is also capable of creating horseshoe SST anomalies, as discussed in Czaja and Frankignoul (2002). Summer is the season when the NAH is shown to precede the winter NAO with the best significance (see Figs. 3 and 4). Figure 11 shows the second MCA mode for IPSL-CM5 when the atmosphere leads the ocean by one month during the summer. The second mode provides the best spatial correlation (0.79) between the SST induced by the atmosphere and the NAH pattern in JJA. It illustrates the atmospheric forcing of a SST similar to the NAH by a dipolar Z500 anomaly, whose largest pole is over the subpolar gyre, so that it somewhat resembles the EAP, or a southward-shifted summer NAO. Note that the first MCA mode, which represents 45% of the squared covariance fraction, show the influence of the NAO, shifted northward, which forces a northward shifted SST-tripole with a large anomaly off the coast of

Newfoundland (not shown).

A similar influence of the atmosphere onto the summer SST is present in the observations, as seen in Fig. 12. The largest spatial correlation between the SST forced by the atmosphere and the NAH SST pattern in MJJ is found for the first MCA mode (r=0.78) between the SST in MJJ and Z500 in AMJ, with the atmospheric pattern resembling the spring NAO of Barston and Lizevey (1987), which differs from the summer NAO described by Folland et al. (2009). The second mode shows a weaker spatial correlation with the NAH SST (r=0.46) and has a weaker squared covariance fraction (22%).

The air-sea interactions in the model are thus realistic, even if the model atmospheric pattern responsible for the NAH SST anomalies are somewhat different. In IPSL-CM5, the EAP is the main driver of the NAH in summer, while it is more similar to the NAO in observations. The influence of the atmosphere onto the subtropical region off Senegal is also underestimated and located too far north in IPSL-CM5, consistent with the MCA results (compare Figs. 12 and 11).

In summary, both the spring–early summer atmosphere and the ocean dynamics can lead to horseshoe-like SST anomalies in the North Atlantic, which drive an atmospheric response. In the following section, we compare these effects.

d. *Comparison of the effects of the atmosphere, AMOC and IGG*

In order to characterize the time evolution of the NAH pattern, we choose the summer SST time series of the first MCA mode at lag 6 when ocean leads (see Figs. 3 and 4), but any projection of the SST on the NAH pattern would provide similar results. The temporal correlations between the NAH time series and (1) the yearly low-pass filtered AMO, (2) the yearly AMOC and gyre indices, when known, (3) the atmospheric variability in spring–early summer, are shown in Fig. 13. The AMOC is represented by AMOC-PC1 and the intergyre gyre variability by the IGG time series. The spring–early summer atmospheric variability is represented by the time series associated with the atmosphere in the MCA, when the atmosphere lead the ocean by 1 month during spring–early summer. It corresponds to the atmospheric patterns shown in Figs. 11 and 12. The statistical significance of the correlations is computed with a student t-test, and the number of degrees of freedom is estimated as in Bretherton et al. (1999), except for the AMO, where the time series are sampled at half the filter cut-off period before estimating the number of degrees of freedom as in Bretherton et al. (1999).

In IPSL-CM5 (Fig. 13, upper-left), the NAH is clearly related to the AMO, with a maximum correlation when in phase, consistent with the similarity in their spatial pattern, but showing that the NAH and the AMO have similar low-frequency variability. The observations (Fig. 13, upper-right) show a similar positive and even more persistent correlation between the NAH and the AMO. On the other hand, the spring/summer atmospheric variability only shows a significant positive correlation when in phase with the NAH, similar in the model ($r = 0.46$) and observations ($r = 0.42$). Since there are no significant lagged correlations when NAH lags, the NAH driven by the atmosphere has limited persistence and behaves as a white noise.

When in phase, the AMOC in IPSL-CM5 has a negative correlation with the NAH (Fig. 13, lower-left). Indeed, the atmospheric forcing directly influences both the NAH and the AMOC, as a positive NAO causes a NAH with a negative polarity with our convention, and also weakly enhances the AMOC. A stronger positive correlation is also found when the AMOC leads the NAH, peaking at a lag of about 9 yr. The correlation between the AMOC and the NAH remains significant from lag 5 to lag 13, reflecting a rather low-frequency influence. Since the NAH influences the NAO, this confirms that the low-frequency variability of the AMOC has an impact onto the atmosphere, as shown by Gastineau and Frankignoul (2011). A significant negative correlation is also seen when the AMOC leads the NAH by about 20 years, reflecting the change of phase associated with the strong 20-yr cycle of the AMOC.

The IGG index also shows significant links with the NAH in IPSL-CM5, with a negative correlation while in phase and positive correlation when the IGG leads by a time lag between 4 and 9 years. There is also a significant negative correlation when the IGG leads by 15-23 years, which presumably also reflects the 20-yr periodicity that is seen in many oceanic variables in IPSL-CM5 (Escudier et al. 2012). To briefly document the links between the IGG and the AMOC, Figure 13 (lower-right) shows the temporal correlation between AMOC-PC1 and IGG. The IGG precedes the AMOC by 3 to 11 years, which is consistent with the 5-yr lag between the subpolar influence on the IGG and the AMOC discussed in Escudier et al. (2012). No significant correlation is found when the AMOC leads, so that the delayed effects onto the NAH of the AMOC (lag 9) and that of IGG (lag 5) are well distinct. Since the lag correlation with the AMOC is substantially larger than with the IGG, the AMOC seems to be the dominant driver of the NAH.

5. Discussion and conclusion

The ocean-atmosphere coupling in the North Atlantic region is investigated in the IPSL-CM5 model and observations with a MCA between the SST and the 500-hPa geopotential height. The model results are compared to observations of the 20th century, after the global warming pattern is removed using a linear inverse modeling method. In both model and observations, the main patterns of covariability are given by the NAO and the SST tripole when the atmosphere leads, and by similar NAH SST pattern and a NAO-like pattern when the ocean leads. The SST influence is twice weaker in IPSL-CM5, but it is significant during the whole cold season, while the SST influence is only detected during early winter for the observations, which may, in part, reflects the longer sample in the model and the observational uncertainties. Both in IPSL-CM5 and the observations, the SST anomalies exert a positive feedback on the NAO variability since the tripole and the NAH patterns are rather similar. The NAH pattern in the observation has been related to the stochastic variability of the atmosphere during summer (Czaja and Frankignoul 2002). Here, we show that the NAH pattern also has a significant decadal and multidecadal variability, which is closely related to the AMO.

In the IPSL-CM5 model, an AMOC intensification causes an increase of the northward oceanic heat transport, which warms the temperatures in the North Atlantic region. Therefore, the AMOC, which largely drives the AMO, is also a driver of the NAH, the AMOC leading both the NAH and the AMO by 9 yr. As the summer NAH is followed in winter by an atmospheric response resembling a negative NAO phase, the AMOC-induced warming has a significant impact on the winter NAO activity, favoring a negative NAO state as found by Gastineau and Frankignoul (2011). The AMOC was also found to be a main driver of the AMO in other climate models (e.g. Knight et al. 2005; Danabasoglu 2008; Marini and Frankignoul 2012). Therefore, we suggest a possible influence of the AMOC onto the NAH and NAO during the 20th century, although no direct AMOC observations are available to verify such link. Since the AMOC may be predictable up to a decade ahead (Collins et al. 2006), the AMOC influence onto the NAO implies a potential decadal predictability of the NAO. This may explain the predictability found over the North Atlantic region in the decadal forecast experiments (Pohlmann et al. 2006; Keenlyside et al. 2008; Teng et al. 2011).

The AMOC is a two dimensional view of a more complex three dimensional oceanic circulation, and the meridional overturning is not the only process that influences the NAH even though it appears to be the dominant one. In IPSL-CM5, an intergyre gyre that is forced by the NAO also explains part of the NAH SST anomalies, similarly to the studies of Czaja and Marshall (2001); Bellucci et al. (2008). Interestingly, the intergyre gyre leads to a delayed damping of the SST anomalies that are directly generated by the NAO, with a delay of 4 to 9 years, which is consistent with the time scale of Rossby wave propagation through the Atlantic Basin. The water-mass pathways and their influence on SST need further investigations to reveal the processes involved in the AMOC and gyre circulation and their links.

The role of sea ice in the coupling between ocean and atmosphere was not discussed. Previous studies suggest that sea ice variability acts as a negative feedback on the NAO, as the sea-ice anomaly pattern driven by a positive NAO tends to generate a negative NAO-like atmospheric response (Magnusdottir et al. 2004; Deser et al. 2007; Strong et al. 2009). As the sea-ice extension is too large is IPSL-CM5 (Dufresne et al. 2012), the sea-ice variations take place in unrealistic locations and their impact should be different. Gastineau and Frankignoul (2011) suggested that the AMOC primarily influences the atmosphere in the model via SST changes, not sea-ice changes, but the issue requires further studies.

The IPSL-CM5 simulation presented in this study uses a low resolution. Chelton and Xie (2010) have shown that low-resolution atmospheric GCMs strongly underestimate the ocean-atmosphere coupling due to the poor representation of SST fronts and their impact onto the atmosphere. This may explain in part the low sensitivity of the model response compared to the observations. A better understanding of the ocean-atmosphere interactions will be needed as the resolution of the models increases.

APPENDIX

The removal of ENSO from North Atlantic SST and geopotential height

The variability of ENSO is assessed using the first two PCs of the SST in the equatorial Pacific Ocean (12.5°S-12.5°N, 100°E-80°W). The first (second) modes represent between 62% and 66% (7% and 11%) of the total variance depending on the season. The ENSO variability is rather low in IPSL-CM5, with an incorrect phase locking of the ENSO variability to the annual cycle, even if its frequency spectrum is relatively similar to that of the observations (Kamala et al. 2012).

Here, the relations between ENSO and the North Atlantic variability are assessed using simultaneous regressions of the SST (K) and Z500 (m) onto the first normalized PC of the Equatorial Pacific SST. In observations (Fig. 14), the main ENSO effect is to shift the subtropical jets equatorwards during El Niño phase, thereby inducing the same SST anomalies as a negative NAO in the Atlantic subtropical domain (Seager et al. 2003), while the subpolar North Atlantic SST anomalies are much weaker and not significant. In IPSL-CM5 (Fig. 15), the subtropical SST anomalies in response to ENSO are weaker, which is consistent with an underestimation of the SST variability off the coast of Africa. A positive phase of ENSO (El Niño) also tends to warm the subpolar gyre, and the overall SST pattern is similar to the SST tripole associated to a negative NAO. This is consistent with the AMO (see Fig. 5, lower panels), that shows a link between the North Atlantic subpolar region and the equatorial Pacific Ocean in IPSL-CM5, but not for HadISST-LIM. This might be related to the incorrect phase locking of ENSO, which was demonstrated to alter the teleconnection with the Equatorial Pacific (Kamala et al. 2012).

The winter Z500 related to ENSO SST anomalies has strong anomalies over North America, as the Pacific-North American pattern is strongly modulated by ENSO. Over the North Atlantic the Z500 anomalies are roughly similar to the NAO, an El Niño phase causing a negative phase of the NAO in both model and observation as in Alexander and Scott (2002). The anomalies are also similar to those of OrtizBeviá et al. (2010), but the strong non-linearity of the ENSO teleconnections is neglected in this study.

In both the model and observations, ENSO has an impact onto SST and Z500 similar to the local influence of SST anomalies (compare Figs. 14 and 15 with Figs. 3 and 4, for lags larger than 3 and 4 months). Unlike in the observations of Frankignoul and Kestenare (2005), the removal of ENSO turned out to reduce the statistical significance of squared covariance and correlation of the first MCA mode when the ocean leads compared to other studies Czaja and Frankignoul (1999, 2002), where ENSO was not removed from the SST and Z500. For example, when ENSO is not removed in observations, the squared covariance of the first MCA mode is 5% significant up to lag 6 months when the ocean leads for the FMA atmosphere, while the statistical significance is similar for the NDJ atmosphere.

Acknowledgments.

The research leading to these results has received funding from the European Community's 7th framework programme (FP7/2007-2013) under grant agreement No. GA212643 (THOR: "Thermohaline Overturning — at Risk", 2008-2012). We are grateful to C. Marini who provided the HadISST-LIM data. We also thank J. Mignot, D. Swingedouw and two anonymous reviewers for their useful comments and suggestions.

REFERENCES

Alexander, M. and J. Scott, 2002: The influence of ENSO on air-sea interaction in the Atlantic. *Geophys. Res. Lett.*, **29 (14)**, 46, doi:10.1029/2001GL014347.

Barston, A. G. and R. E. Lizevey, 1987: Classification, seasonality and persistence of low-frequency atmospheric circulation patterns. *Mon. Wea. Rev.*, **115**, 1083–1126.

Bellucci, A., S. Gualdi, E. Scoccimarro, and A. Navarra, 2008: NAO-ocean circulation interactions in a coupled general circulation model. *Clim. Dyn.*, **31 (7)**, 759–777.

Bretherton, C., M. Widmann, V. Dymnikov, J. Wallace, and I. Bladé, 1999: The effective number of spatial degrees of freedom of a time-varying field. *J. Climate*, **12 (7)**, 1990–2009.

Bretherton, C. S., C. Smith, and J. M. Wallace, 1992: An intercomparison of methods for finding coupled patterns in climate data. *J. Climate*, **5 (6)**, 541–560.

Cassou, C., C. Deser, and M. A. Alexander, 2007: Investigating the impact of reemerging sea surface temperature anomalies on the winter atmospheric circulation over the North Atlantic. *J. Climate*, **20 (14)**, 3510–3526.

Cayan, D. R., 1992: Latent and sensible heat flux anomalies over the northern oceans: the connection to monthly atmospheric circulation. *J. Climate*, **5 (4)**, 354–369.

Chelton, D. and S.-P. Xie, 2010: Coupled ocean-atmosphere interaction at oceanic mesoscales. *Oceanography*, **23 (4)**, 52–69.

Collins, M., et al., 2006: Interannual to decadal climate predictability in the North Atlantic: a multimodel-ensemble study. *J. Climate*, **19 (7)**, 1195–1203.

Compo, G. P. and P. D. Sardeshmukh, 2010: Removing ENSO-related variations from the climate record. *J. Climate*, **23 (8)**, 1957–1978.

Compo, G. P., et al., 2011: The twentieth century reanalysis project. *Q. J. R. Meteorol. Soc.*, **137 (654)**, 1–28.

Cunningham, S. A., et al., 2007: Temporal variability of the Atlantic Meridional Overturning Circulation at 26.5N. *Science*, **317 (5840)**, 935–938.

Czaja, A. and C. Frankignoul, 1999: Influence of the North Atlantic SST on the atmospheric circulation. *Geophys. Res. Lett.*, **26**, 2969–2972.

Czaja, A. and C. Frankignoul, 2002: Observed impact of Atlantic SST anomalies on the North Atlantic oscillation. *J. Climate*, **15 (6)**, 606–623.

Czaja, A. and J. Marshall, 2001: Observations of atmosphere-ocean coupling in the North Atlantic. *Q. J. R. Meteorol. Soc.*, **127**, 1893–1916.

Czaja, A., P. van der Vaart, and J. Marshall, 2002: A diagnostic study of the role of remote forcing in tropical Atlantic variability. *J. Climate*, **15 (22)**, 3280–3290.

Danabasoglu, G., 2008: On multidecadal variability of the Atlantic meridional overturning circulation in the Community Climate System Model version 3. *J. Climate*, **21 (21)**, 5524–5544.

D'Andrea, F., A. Czaja, and J. Marshall, 2005: Impact of anomalous ocean heat transport on the North Atlantic oscillation. *J. Climate*, **18 (23)**, 4955–4969.

Delworth, T. L. and R. J. Greatbatch, 2000: Multidecadal thermohaline circulation variability driven by atmospheric surface flux forcing. *J. Climate*, **13 (9)**, 1481–1495.

Deser, C., M. A. Alexander, S. Xie, and A. S. Phillips, 2009: Sea surface temperature variability: patterns and mechanisms. *Annu. Rev. Marine. Sci.*, **2 (1)**, 115–143.

Deser, C., R. A. Tomas, and S. Peng, 2007: The transient atmospheric circulation response to North Atlantic SST and sea ice anomalies. *J. Climate*, **20 (18)**, 4751–4767.

Deshayes, J. and C. Frankignoul, 2008: Simulated variability of the circulation in the North Atlantic from 1953 to 2003. *J. Climate*, **21 (19)**, 4919–4933.

Dong, B., R. T. Sutton, and A. A. Scaife, 2006: Multidecadal modulation of El Niño Southern Oscillation (ENSO) variance by Atlantic Ocean sea surface temperatures. *Geophys. Res. Lett.*, **33 (8)**, L08 705, doi: 10.1029/2006GL025766.

Dufresne, J.-L., et al., 2012: Climate change projections using the IPSL-CM5 Earth System Model: from CMIP3 to CMIP5. *Clim. Dyn. submitted*.

Eden, C. and R. J. Greatbatch, 2003: A damped decadal oscillation in the North Atlantic climate system. *J. Climate*, **16 (24)**, 4043–4060.

Eden, C. and J. Willebrand, 2001: Mechanism of interannual to decadal variability of the North Atlantic circulation. *J. Climate*, **14 (10)**, 2266–2280.

Enfield, D. B. and L. Cid-Serrano, 2010: Secular and multidecadal warmings in the North Atlantic and their relationships with major hurricane activity. *Int. J. Climatol.*, **30 (2)**, 174–184.

Escudier, R., J. Mignot, and D. Swingedouw, 2012: A 20-yr coupled ocean-sea ice-atmosphere variability mode in the North Atlantic in an AOGCM. *Clim. Dyn. submitted*.

Feldstein, S. B., 2000: The timescale, power spectra, and climate noise properties of teleconnection patterns. *J. Climate*, **13 (24)**, 4430–4440.

Folland, C. K., J. Knight, H. W. Linderholm, D. Fereday, S. Ineson, and J. W. Hurrell, 2009: The summer North Atlantic oscillation: past, present, and future. *J. Climate*, **22 (5)**, 1082–1103.

Frankignoul, C., N. Chouaib, and Z. Liu, 2011: Estimating the observed atmospheric response to SST anomalies: Maximum covariance analysis, generalized equilibrium feedback assessment, and maximum response estimation. *J. Climate*, **24 (10)**, 2523–2539, doi:10.1175/2010JCLI3696.1.

Frankignoul, C. and K. Hasselmann, 1977: Stochastic climate models. Part II: application to sea-surface temperature anomalies and thermocline variability. *Tellus*, **29 (4)**, 289–305.

Frankignoul, C. and E. Kestenare, 2002: The surface heat flux feedback. Part I: estimates from observations in the Atlantic and the North Pacific . *Clim. Dyn.*, **19**, 633–647.

Frankignoul, C. and E. Kestenare, 2005: Air-sea interactions in the tropical Atlantic: a view based on lagged rotated maximum covariance analysis. *J. Climate*, **18 (18)**, 3874–3890.

Gastineau, G. and C. Frankignoul, 2011: Cold-season atmospheric response to the natural variability of the Atlantic meridional overturning circulation. *Clim. Dyn., in press*, 1–21, doi:10.1007/s00382-011-1109-y.

Gray, S. T., L. J. Graumlich, J. L. Betancourt, and G. T. Pederson, 2004: A tree-ring based reconstruction of the Atlantic multidecadal oscillation since 1567 A.D. *Geophys. Res. Lett.*, **31 (12)**, L12 205, doi:10.1029/2004GL019932.

Guan, B. and S. Nigam, 2009: Analysis of Atlantic SST variability factoring interbasin links and the secular trend: clarified structure of the Atlantic multidecadal oscillation. *J. Climate*, **22 (15)**, 4228–4240.

Guemas, V. and F. Codron, 2011: Differing impacts of resolution changes in latitude and longitude on the midlatitudes in the LMDZ atmospheric GCM. *J. Climate*, **24 (22)**, 5831–5849.

Hodson, D., R. Sutton, C. Cassou, N. Keenlyside, Y. Okumura, and T. Zhou, 2010: Climate impacts of recent multidecadal changes in Atlantic Ocean sea surface temperature: a multimodel comparison. *Clim. Dyn.*, **34**, 1041–1058.

Hourdin, F., et al., 2012a: Climate and sensitivity of the IPSL-CM5A coupled model: impact of the LMDZ atmospheric grid configuration. *Clim. Dyn. submitted*.

Hourdin, F., et al., 2012b: From LMDZ5A to LMDZ5B : revisiting the parameterizations of clouds and convection in the atmospheric component of the IPSL-CM5 climate model. *Clim. Dyn. submitted*.

Hurrell, J., Y. Kushnir, M. Visbeck, and G. Ottersen, 2003: An overview of the North Atlantic oscillation. *The North Atlantic oscillation, climatic significance and environmental impact, AGU Geophysical Monograph*, **134**, 1–35.

Kamala, K., Y. Peings, P. Terray, and H. Douville, 2012: ENSO-Indian monsoon teleconnection in the CNRM and IPSL historical simulations. *Clim. Dyn. submitted*.

Keenlyside, N., M. Latif, J. Jungclaus, L. Kornblueh, and E. Roeckner, 2008: Advancing decadal-scale climate prediction in the North Atlantic sector. *Nature*, **453**, 84–88.

Knight, J., R. Allan, C. Folland, M. Vellinga, and M. Mann, 2005: A signature of persistent natural thermohaline circulation cycles in observed climate. *Geophys. Res. Lett.*, **32**, L20 708, doi: 1029/2005GL024 233.

Krinner, G., et al., 2005: A dynamic global vegetation model for studies of the coupled atmosphere-biosphere system. *Global Biogeochem. Cycles*, **19 (1)**, GB1015, doi:10.1029/2003GB002199.

Kushnir, Y., 1994: Interdecadal variations in North Atlantic sea surface temperature and associated atmospheric conditions. *J. Climate*, **7 (1)**, 141–157.

Madec, G., P. Delecluse, M. Imbard, and M. Levy, 1998: OPA 8.1, ocean general circulation model reference manual. Tech. rep., LOCEAN/IPSL. Note du Pole de modelisation, Institut Pierre-Simon Laplace, No 11, pp99.

Magnusdottir, G., C. Deser, and R. Saravanan, 2004: The effects of North Atlantic SST and sea ice anomalies on the winter circulation in CCM3. Part I: main features and storm track characteristics of the response. *J. Climate*, **17 (5)**, 857–876.

Mann, M. E., R. S. Bradley, and M. K. Hughes, 1998: Global-scale temperature patterns and climate forcing over the past six centuries. *Nature*, **392 (6678)**, 779–787.

Marini, C. and C. Frankignoul, 2012: Deconstructing the Atlantic multidecadal oscillation. *J. Clim., submitted*.

Marshall, J., H. Johnson, and J. Goodman, 2001: A study of the interaction of the North Atlantic oscillation with ocean circulation. *J. Climate*, **14 (7)**, 1399–1421.

Maury, P., F. Lott, L. Guez, and J.-P. Duvel, 2012: Tropical variability and stratospheric equatorial waves in the IPSLCM5 model. *Clim. Dyn. submitted*.

Medhaug, I. and T. Furevik, 2011: North Atlantic 20th century multidecadal variability in coupled climate models: sea surface temperature and ocean overturning circulation. *Ocean Sci.*, **7**, 389–404, doi:10.5194/os-7-389-2011.

Msadek, R. and C. Frankignoul, 2009: Atlantic multidecadal oceanic variability and its influence on the atmosphere in a climate model. *Clim. Dyn.*, **33**, 45–62.

Munoz, E., B. Kirtman, and W. Weijer, 2011: Varied representation of the Atlantic meridional overturning across multidecadal ocean reanalyses. *Deep Sea Res. II*, **58 (17-18)**, 1848–1857.

OrtizBeviá, M. J., I. Pérez-González, F. J. Alvarez-García, and A. Gershunov, 2010: Nonlinear estimation of El Niño impact on the North Atlantic winter. *J. Geophys. Res.*, **115**, D21 123, doi:10.1029/2009JD013387.

Park, S., C. Deser, and M. A. Alexander, 2005: Estimation of the surface heat flux response to sea surface temperature anomalies over the global oceans. *J. Climate*, **18 (21)**, 4582–4599.

Peng, S., W. A. Robinson, and S. Li, 2002: North Atlantic SST forcing of the NAO and relationships with intrinsic hemispheric variability. *Geophys. Res. Lett.*, **29 (8)**, 1276, doi:10.1029/2001GL014043.

Peng, S., W. A. Robinson, and S. Li, 2003: Mechanisms for the NAO responses to the North Atlantic SST tripole. *J. Climate*, **16 (12)**, 1987–2004.

Peng, S. and J. S. Whitaker, 1999: Mechanisms determining the atmospheric response to midlatitude SST anomalies. *J. Climate*, **12 (5)**, 1393–1408.

Penland, C. and L. Matrosova, 2006: Studies of El Niño and interdecadal variability in tropical sea surface temperatures using a nonnormal filter. *J. Climate*, **19 (22)**, 5796–5815.

Pohlmann, H., F. Sienz, and M. Latif, 2006: Influence of the multidecadal Atlantic meridional overturning circulation variability on European climate. *J. Climate*, **19 (23)**, 6062–6067.

Quadrelli, R. and J. M. Wallace, 2004: A simplified linear framework for interpreting patterns of northern hemisphere wintertime climate variability. *J. Climate*, **17 (19)**, 3728–3744.

Rayner, N. A., D. E. Parker, E. B. Horton, C. K. Folland, L. V. Alexander, D. P. Rowell, E. C. Kent, and A. Kaplan, 2003: Global analyses of sea surface temperature, sea ice, and night marine air temperature since the late nineteenth century. *J. Geophys. Res.*, **108 (D14)**, 4407, doi:10.1029/2002JD002670.

Schneider, E. K. and M. Fan, 2012: Observed decadal North Atlantic tripole SST variability. Part II: diagnosis of mechanisms. *J. Atmos. Sci.*, **69 (1)**, 51–64.

Schott, F. A., T. N. Lee, and R. Zantopp, 1988: Variability of structure and transport of the Florida current in the period range of days to seasonal. *J. Phys. Oceanogr.*, **18 (9)**, 1209–1230.

Seager, R., N. Harnik, Y. Kushnir, W. Robinson, and J. Miller, 2003: Mechanisms of hemispherically symmetric climate variability. *J. Climate*, **16**, 2960–2978.

Sevellec, F. and A. Fedorov, 2012: An interdecadal oscillatory eigenmode of the Atlantic meridional overturning circulation in a realistic ocean GCM. *J. Clim., submitted*.

Stickler, A., et al., 2009: The comprehensive historical Upper-Air network. *Bull. Am. Meteorol. Soc.*, **91 (6)**, 741–751.

Strong, C., G. Magnusdottir, and H. Stern, 2009: Observed feedback between winter sea ice and the North Atlantic oscillation. *J. Climate*, **22 (22)**, 6021–6032.

Sutton, R. T. and D. L. R. Hodson, 2007: Climate response to basin-scale warming and cooling of the North Atlantic Ocean. *J. Climate*, **20 (5)**, 891–907.

Sutton, R. W. and D. L. R. Hodson, 2005: Atlantic Ocean forcing of North American and European summer climate. *Science*, **309**, 115–118.

Teng, H., G. Branstator, and G. A. Meehl, 2011: Predictability of the Atlantic overturning circulation and associated surface patterns in two CCSM3 climate change ensemble experiments. *J. Climate, in press*, doi:10.1175/2011JCLI4207.1.

Thompson, D. and J. Wallace, 1998: The Arctic oscillation signature in the wintertime geopotential height and temperature fields. *Geophys. Res. Lett.*, **25**, 1297–1300.

Trenberth, K. E. and D. J. Shea, 2006: Atlantic hurricanes and natural variability in 2005. *Geophys. Res. Lett.*, **33**, L12 704, doi:10.1029/2006GL026 894.

Valcke, S., 2006: OASIS3 User guide (prism 2-5). Tech. rep., CERFACS. PRISM Support Initiative Report, No 3, pp64.

Watanabe, M. and M. Kimoto, 2000: Atmosphere-ocean thermal coupling in the North Atlantic: a positive feedback. *Q. J. R. Meteorol. Soc.*, **126 (570)**, 3343–3369.

List of Figures

1 First two EOFs, in m, of the winter (JFM) 500-hPa geopotential height (Z500) in IPSL-CM5. The variance fraction is indicated in parentheses. 33

2 Squared covariance (SC) of the first MCA mode between the North Atlantic SST and Z500 anomalies, for (left panel) IPSL-CM5 and (right panel) NCEP 20th century and HadISST-LIM observations. Units are 10^6 m^2 K^2. The grey shades indicate the significance of the SC. 34

3 Heterogeneous (or homogeneous) Z500 (m) in JFM and homogeneous (or heterogeneous) SST (K) covariance maps, for the first MCA mode, in IPSL-CM5. The atmosphere is shown at JFM, the lag (L), in month, is positive when the ocean leads. When the atmosphere leads or in phase, the homogeneous Z500 and heterogeneous SST are shown. When the ocean leads, the heterogeneous Z500 and homogeneous SST are shown. The squared covariance (SC) in 10^6 m^2 K^2, the correlation (R) and their respective significance in % are indicated above each panel. The squared covariance fraction (SCF) is also indicated. Note that the contour interval is different for the homogeneous (10 m) and heterogeneous (2 m) Z500 maps. SST anomalies all uses the color bar. 35

4 Same as Fig. 3, but for the NCEP 20th century reanalysis and HadSST-LIM, for Z500 in NDJ. 36

5 (Upper panels) Mean and first EOF of the AMOC, in Sv, in IPSL-CM5. The variance fraction of the first EOF is given in parentheses. (Lower panels) AMO defined by the regression of the 10-yr low pass filtered mean Atlantic SST over 10°N-60°N onto the SST, in IPSL-CM5 and in HadISST-LIM. The same color scale is used for model and observations in the lower panels. 37

6 SST (in K) regression onto normalized AMOC-PC1 in IPSL-CM5, for (left panel) summer (JAS) and (right panel) fall (OND). The lag (in year) is positive when AMOC-PC1 leads. The thick black lines indicate the 5% significance, given by Monte Carlo analysis. 38

7 Spatial correlation between the NAH pattern and the lagged SST regression onto normalized yearly AMOC-PC1 (left panel) and the intergyre gyre index (IGG, right panel), in IPSL-CM5, for (upper panel) JAS and (lower panel) OND. The lag (in year) is positive when AMOC-PC1 or IGG leads. The dashed lines indicate the 5% and 10% significance, given by spatial correlations from an ensemble of randomly scrambled AMOC-PC1 and IGG time series. . . 39

8 Atmospheric response to the AMOC in IPSL-CM5, during winter (JFM), when the AMOC-PC1 leads by 9 years. (Upper-left panel) SST (K) regression onto normalized AMOC-PC1. (Upper-right panel) Total heat flux Q (W m^{-1}) regression onto normalized AMOC-PC1, positive upward. (Lower-left panel) Maximum Eady growth rate at 850-hPa, σ_{BI}, regressed onto normalized AMOC-PC1, in day^{-1}. (Lower-right panel) Storm track activity, in m, shown by the pass-band (2.2-5 days) standard deviation of the 500-hPa geopotential height, $\overline{z'^2_{500}}$, regressed onto normalized AMOC-PC1. Thick black lines show the 5% significance. The mean climatological Q, $\overline{z'^2_{500}}$ and σ_{BI} are shown with thick red contours using 100 W m^{-1} for Q, 20 m for $\overline{z'^2_{500}}$, 0.5 and 0.8 day^{-1} for σ_{BI} as contour interval. Note that all red contours are positive. 40

9 First two EOFs of the yearly barotropic streamfunction, in Sv, in IPSL-CM5. Positive values indicate clockwise circulation. The variance fraction is indicated in the top. 41

10 SST (in K) regression onto the normalized intergyre gyre index (IGG) in IPSL-CM5, for (left panel) summer, JAS, and (right panel) fall, OND. The lag (in year) is positive when IGG leads. The thick black lines indicate the 5% significance, given by Monte Carlo analysis. . . 42

11 Homogeneous Z500 (in m) and heterogeneous SST (in K) of the second MCA mode, when the summer (JAS) atmosphere leads the ocean by one month (L= -1), for IPSL-CM5. The squared covariance (SC) in 10^6 m^2 K^2, the correlation (R), their respective significance in %, and the squared covariance fraction (SCF) are indicated in the top. The color bar refers to SST. 43

12 Same as Fig. 11, but for the first MCA mode, and for the spring–early summer atmosphere (MJJ), in NCEP 20th century and HadISST-LIM. 44

13 (Upper panel) Temporal correlation between the NAH and the atmospheric forcing, and AMO in (left panel) IPSL-CM5 and (right panel) 20th century NCEP reanalysis and HadISST-LIM. (Lower-left panel) Temporal correlation between the NAH and the PC1 of the yearly AMOC (AMOC-PC1) and the intergyre gyre index (IGG) in IPSL-CM5. (Lower-right panel) Temporal correlation between the AMOC-PC1 and the intergyre gyre index (IGG) in IPSL-CM5. The lag is positive (negative) when the NAH lags (leads), except for lower-right panel where it is positive (negative) when the IGG lags (leads). The 5% significance of the correlation for each variable is given with dashed lines. 45

14 Regression of the JFM (left panel) SST, in K, and (right panel) Z500, in m, onto the normalized ENSO index, in NCEP 20th century and HadISST-LIM. The ENSO index is the PC1 of the JFM SST in the Equatorial Pacific. The color shades are suppressed when the significance, given by Monte Carlo analysis, is above 5%. 46

15 Same as Fig. 14, but for IPSL-CM5 during JFM. 47

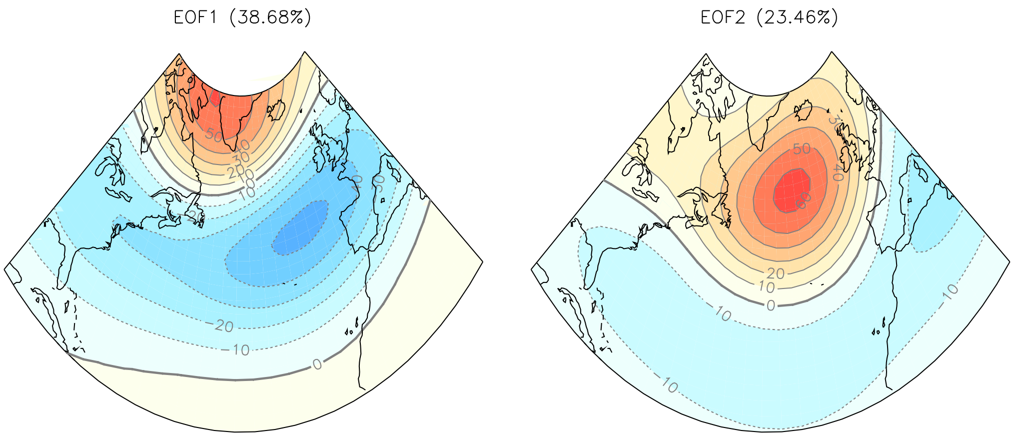

Fig. 1. First two EOFs, in m, of the winter (JFM) 500-hPa geopotential height (Z500) in IPSL-CM5. The variance fraction is indicated in parentheses.

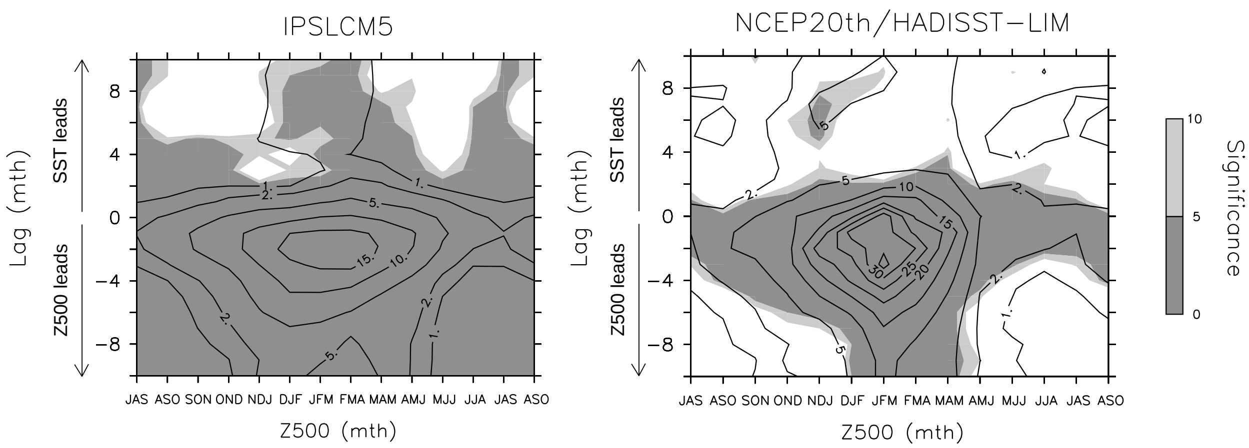

FIG. 2. Squared covariance (SC) of the first MCA mode between the North Atlantic SST and Z500 anomalies, for (left panel) IPSL-CM5 and (right panel) NCEP 20th century and HadISST-LIM observations. Units are 10^6 m^2 K^2. The grey shades indicate the significance of the SC.

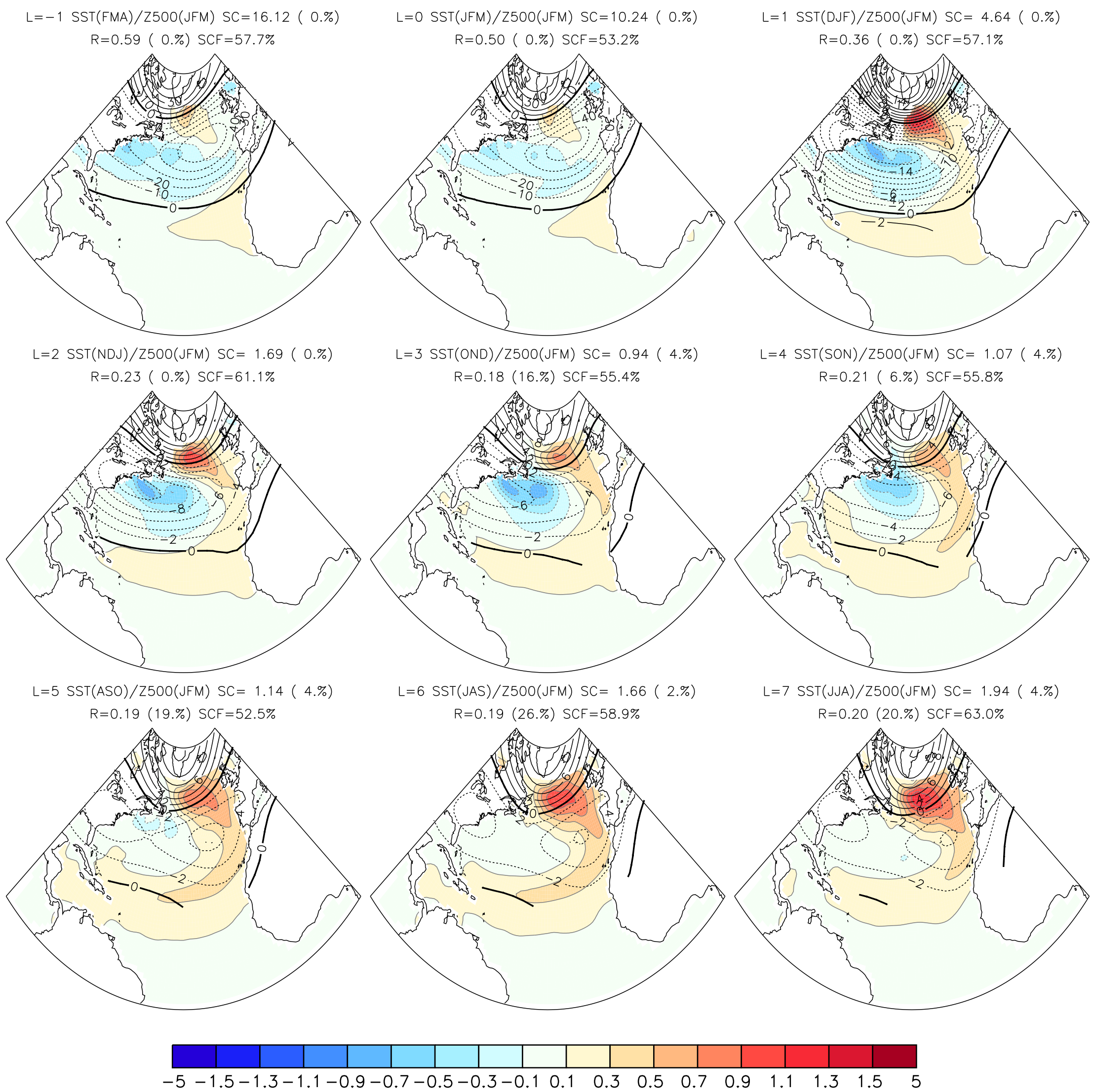

FIG. 3. Heterogeneous (or homogeneous) Z500 (m) in JFM and homogeneous (or heterogeneous) SST (K) covariance maps, for the first MCA mode, in IPSL-CM5. The atmosphere is shown at JFM, the lag (L), in month, is positive when the ocean leads. When the atmosphere leads or in phase, the homogeneous Z500 and heterogeneous SST are shown. When the ocean leads, the heterogeneous Z500 and homogeneous SST are shown. The squared covariance (SC) in 10^6 m^2 K^2, the correlation (R) and their respective significance in % are indicated above each panel. The squared covariance fraction (SCF) is also indicated. Note that the contour interval is different for the homogeneous (10 m) and heterogeneous (2 m) Z500 maps. SST anomalies all uses the color bar.

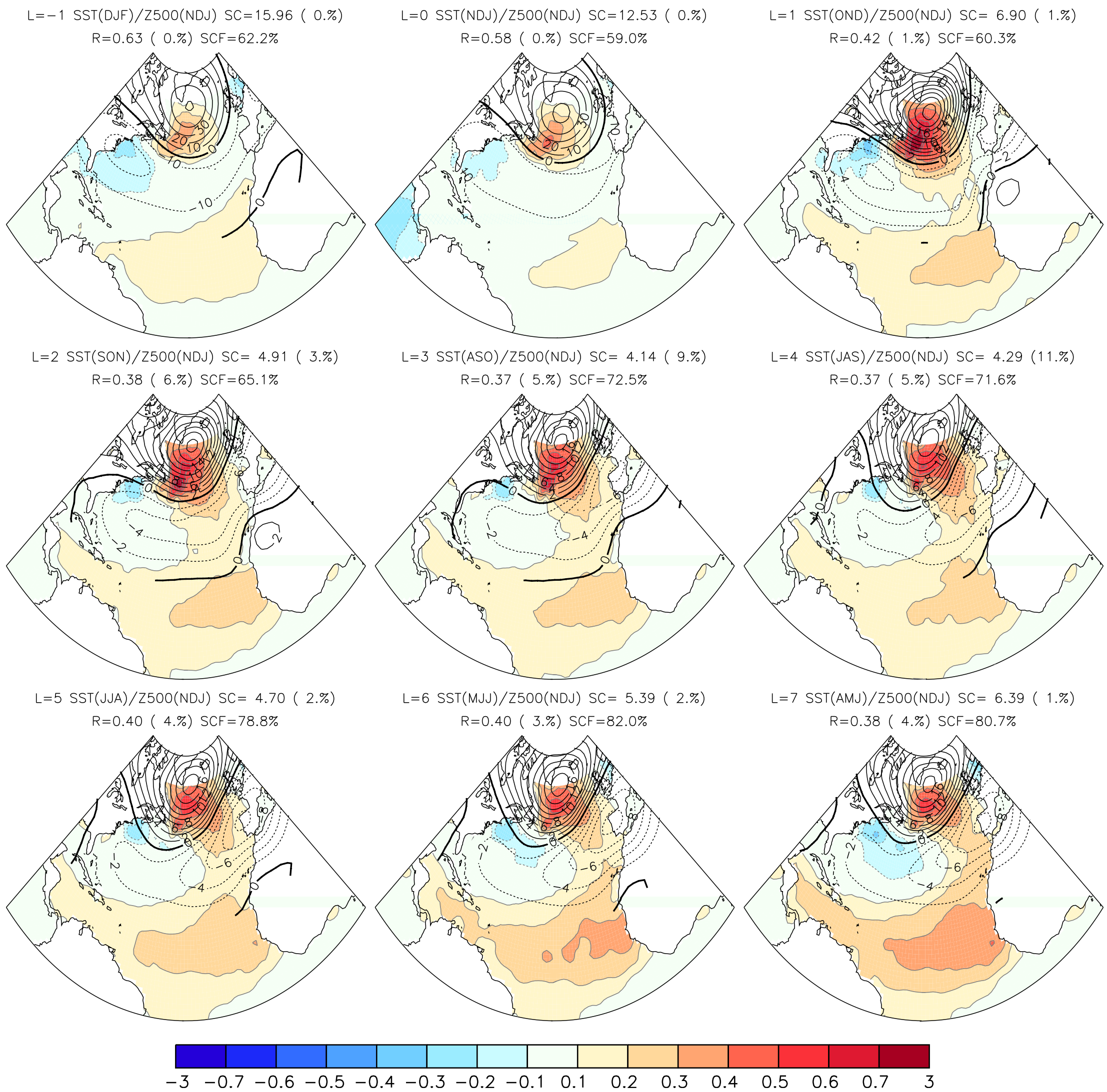

Fig. 4. Same as Fig. 3, but for the NCEP 20th century reanalysis and HadSST-LIM, for Z500 in NDJ.

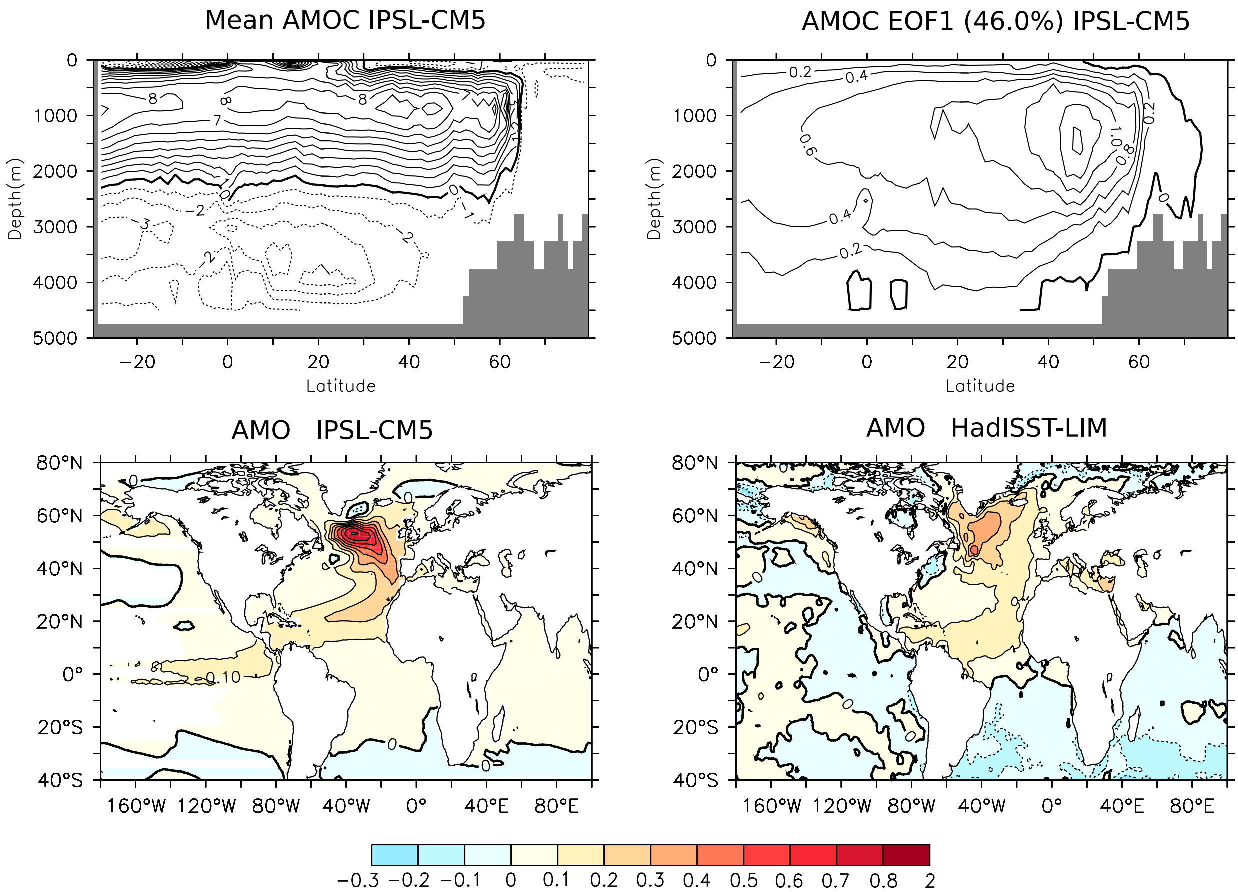

FIG. 5. (Upper panels) Mean and first EOF of the AMOC, in Sv, in IPSL-CM5. The variance fraction of the first EOF is given in parentheses. (Lower panels) AMO defined by the regression of the 10-yr low pass filtered mean Atlantic SST over 10°N-60°N onto the SST, in IPSL-CM5 and in HadISST-LIM. The same color scale is used for model and observations in the lower panels.

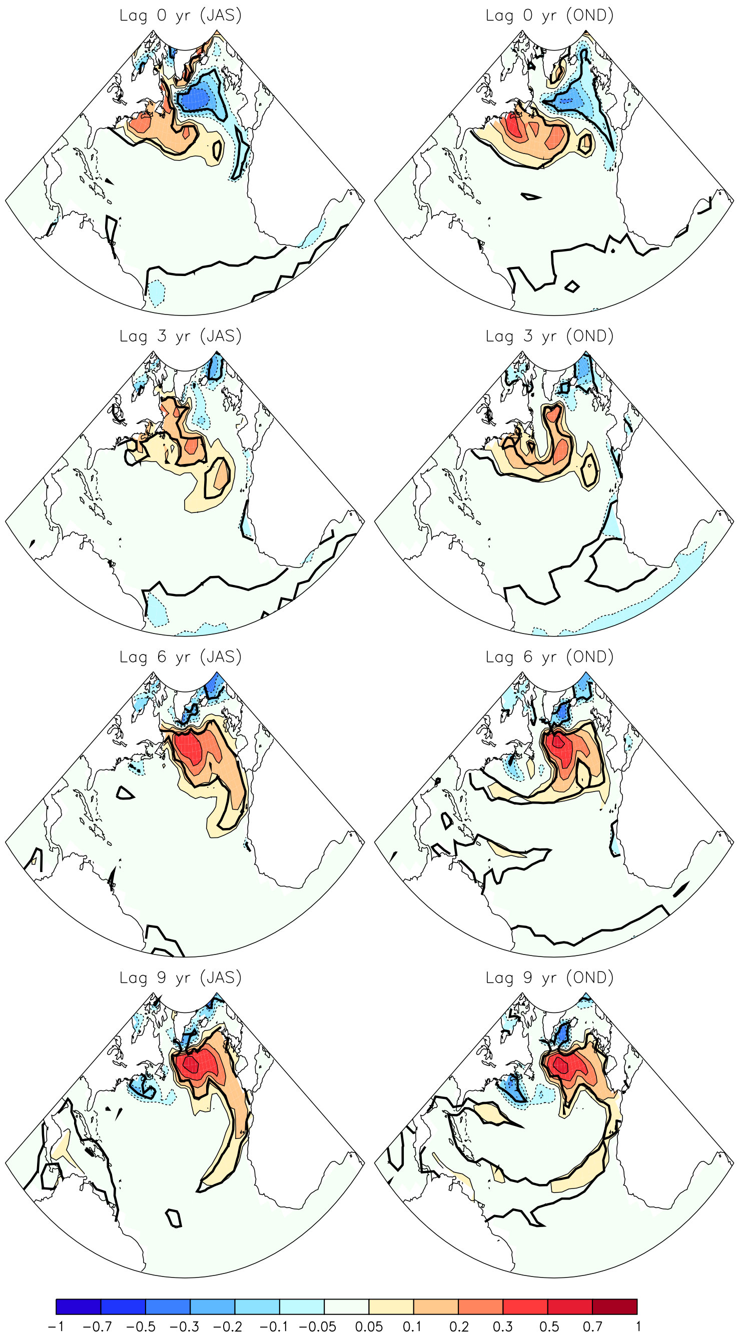

FIG. 6. SST (in K) regression onto normalized AMOC-PC1 in IPSL-CM5, for (left panel) summer (JAS) and (right panel) fall (OND). The lag (in year) is positive when AMOC-PC1 leads. The thick black lines indicate the 5% significance, given by Monte Carlo analysis.

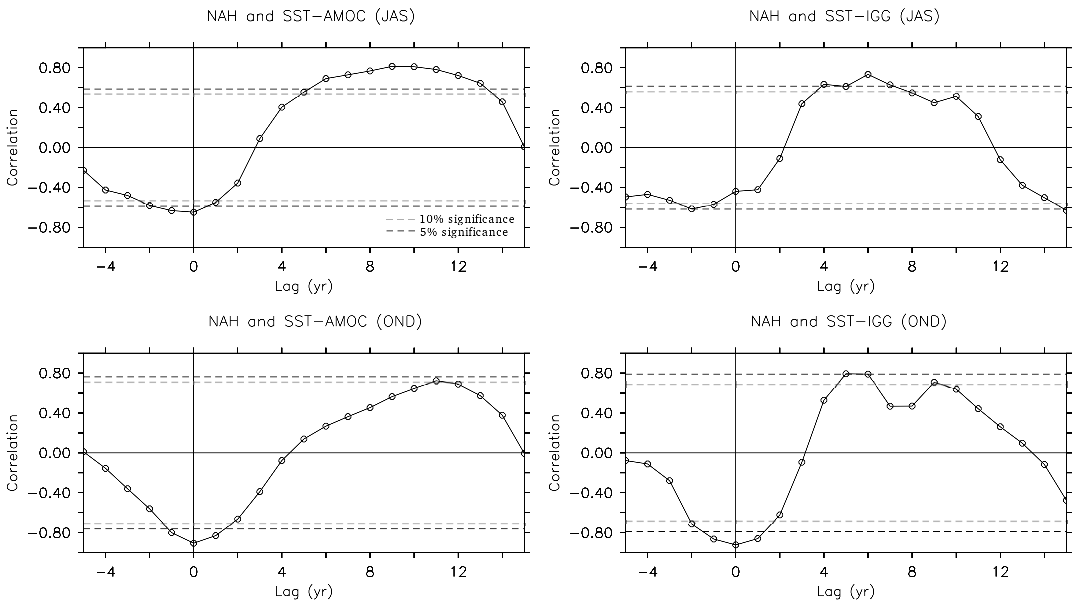

FIG. 7. Spatial correlation between the NAH pattern and the lagged SST regression onto normalized yearly AMOC-PC1 (left panel) and the intergyre gyre index (IGG, right panel), in IPSL-CM5, for (upper panel) JAS and (lower panel) OND. The lag (in year) is positive when AMOC-PC1 or IGG leads. The dashed lines indicate the 5% and 10% significance, given by spatial correlations from an ensemble of randomly scrambled AMOC-PC1 and IGG time series.

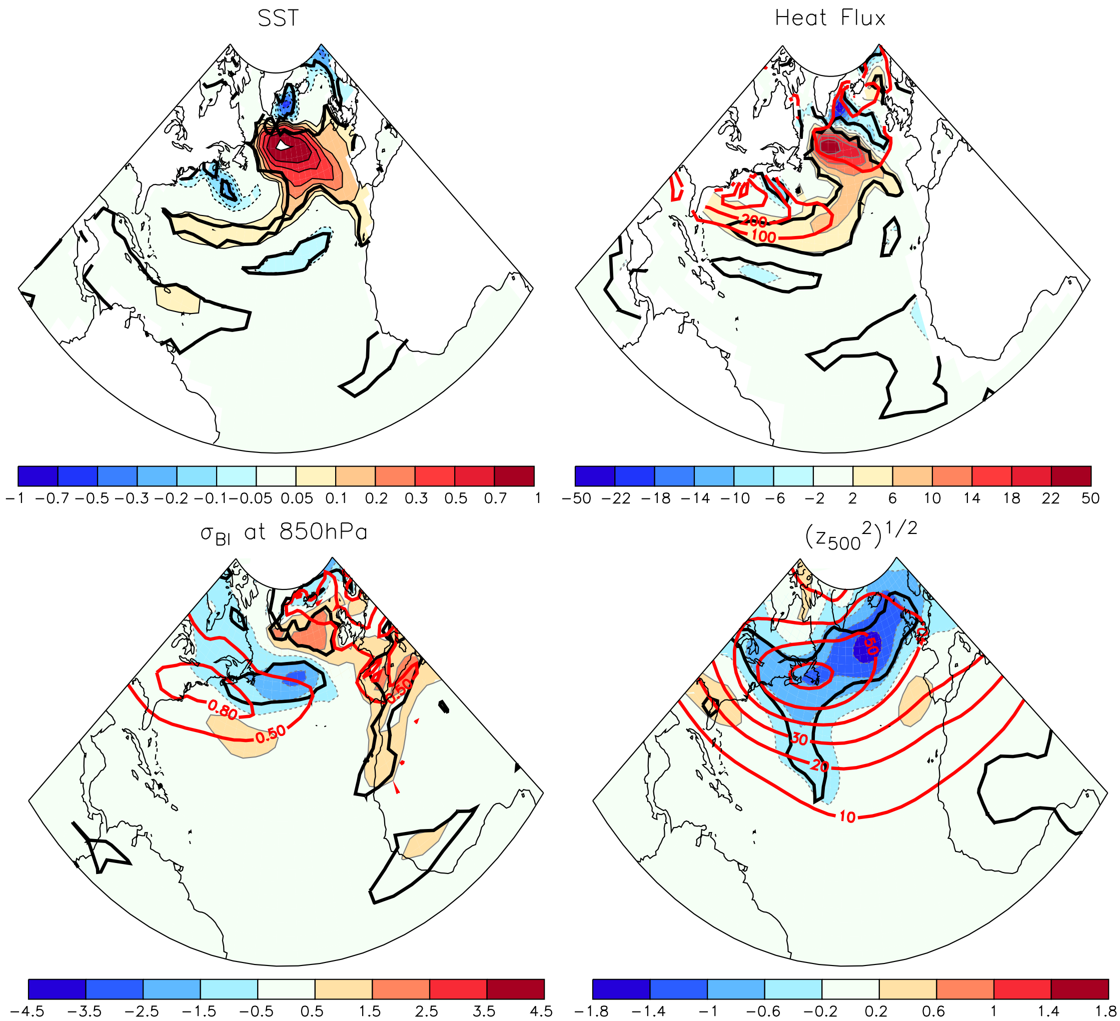

FIG. 8. Atmospheric response to the AMOC in IPSL-CM5, during winter (JFM), when the AMOC-PC1 leads by 9 years. (Upper-left panel) SST (K) regression onto normalized AMOC-PC1. (Upper-right panel) Total heat flux Q (W m^{-1}) regression onto normalized AMOC-PC1, positive upward. (Lower-left panel) Maximum Eady growth rate at 850-hPa, σ_{BI}, regressed onto normalized AMOC-PC1, in day^{-1}. (Lower-right panel) Storm track activity, in m, shown by the pass-band (2.2-5 days) standard deviation of the 500-hPa geopotential height, $\overline{z'^2_{500}}$, regressed onto normalized AMOC-PC1. Thick black lines show the 5% significance. The mean climatological Q, $\overline{z'^2_{500}}$ and σ_{BI} are shown with thick red contours using 100 W m^{-1} for Q, 20 m for $\overline{z'^2_{500}}$, 0.5 and 0.8 day^{-1} for σ_{BI} as contour interval. Note that all red contours are positive.

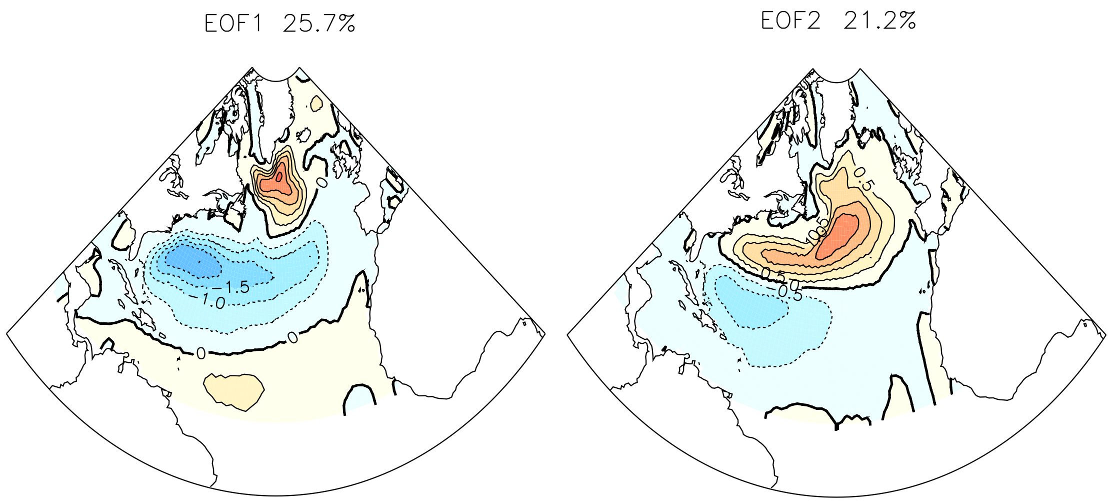

Fig. 9. First two EOFs of the yearly barotropic streamfunction, in Sv, in IPSL-CM5. Positive values indicate clockwise circulation. The variance fraction is indicated in the top.

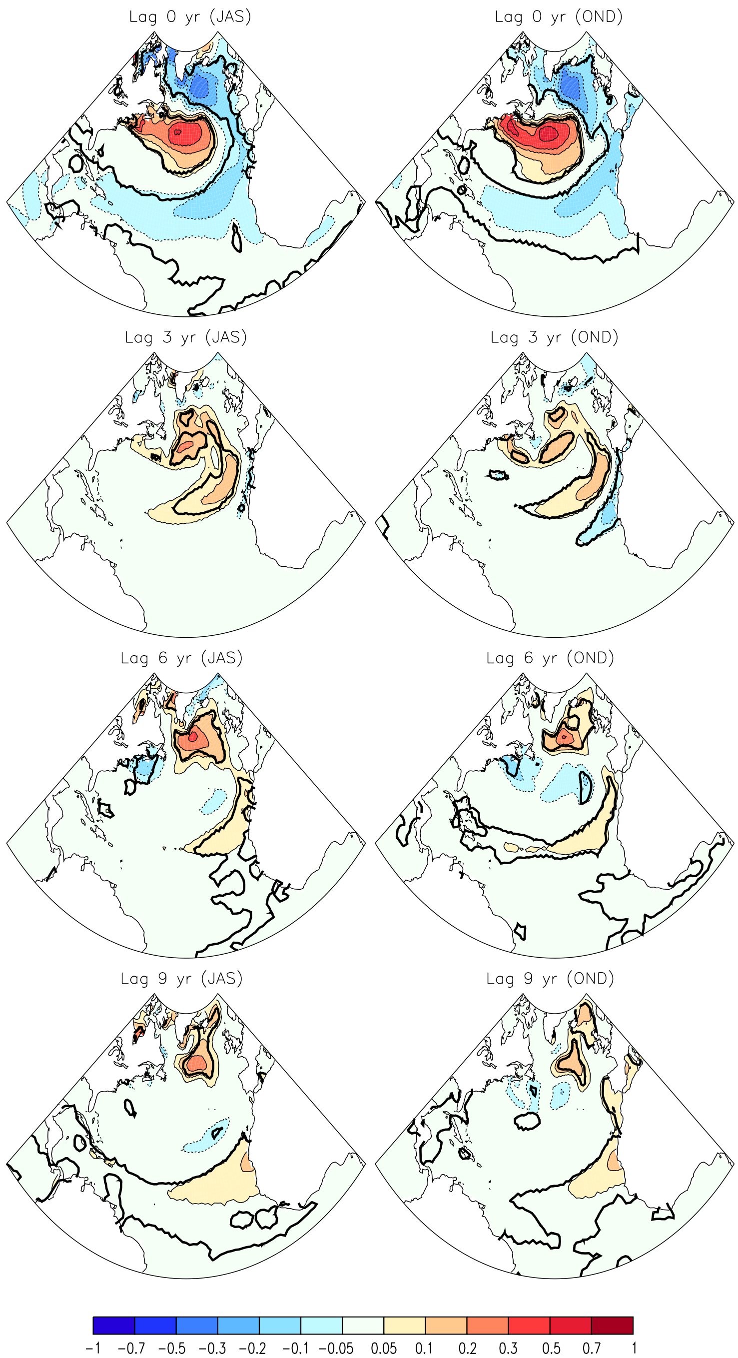

Fig. 10. SST (in K) regression onto the normalized intergyre gyre index (IGG) in IPSL-CM5, for (left panel) summer, JAS, and (right panel) fall, OND. The lag (in year) is positive when IGG leads. The thick black lines indicate the 5% significance, given by Monte Carlo analysis.

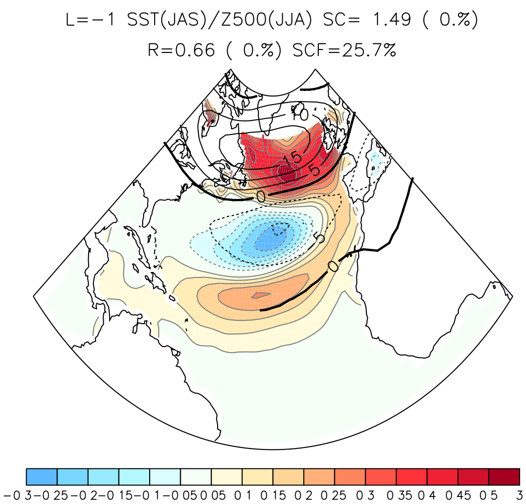

FIG. 11. Homogeneous Z500 (in m) and heterogeneous SST (in K) of the second MCA mode, when the summer (JAS) atmosphere leads the ocean by one month (L= −1), for IPSL-CM5. The squared covariance (SC) in 10^6 m^2 K^2, the correlation (R), their respective significance in %, and the squared covariance fraction (SCF) are indicated in the top. The color bar refers to SST.

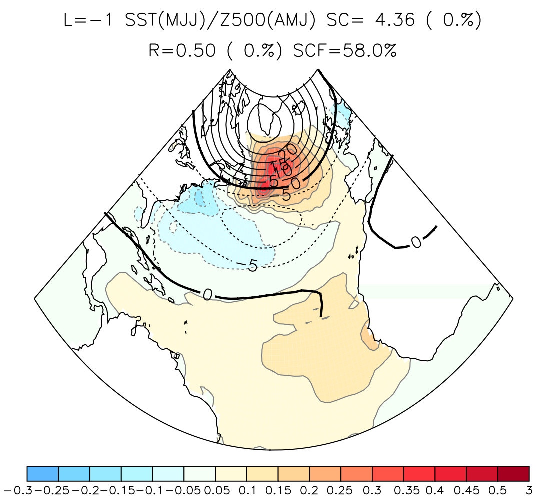

FIG. 12. Same as Fig. 11, but for the first MCA mode, and for the spring–early summer atmosphere (MJJ), in NCEP 20th century and HadISST-LIM.

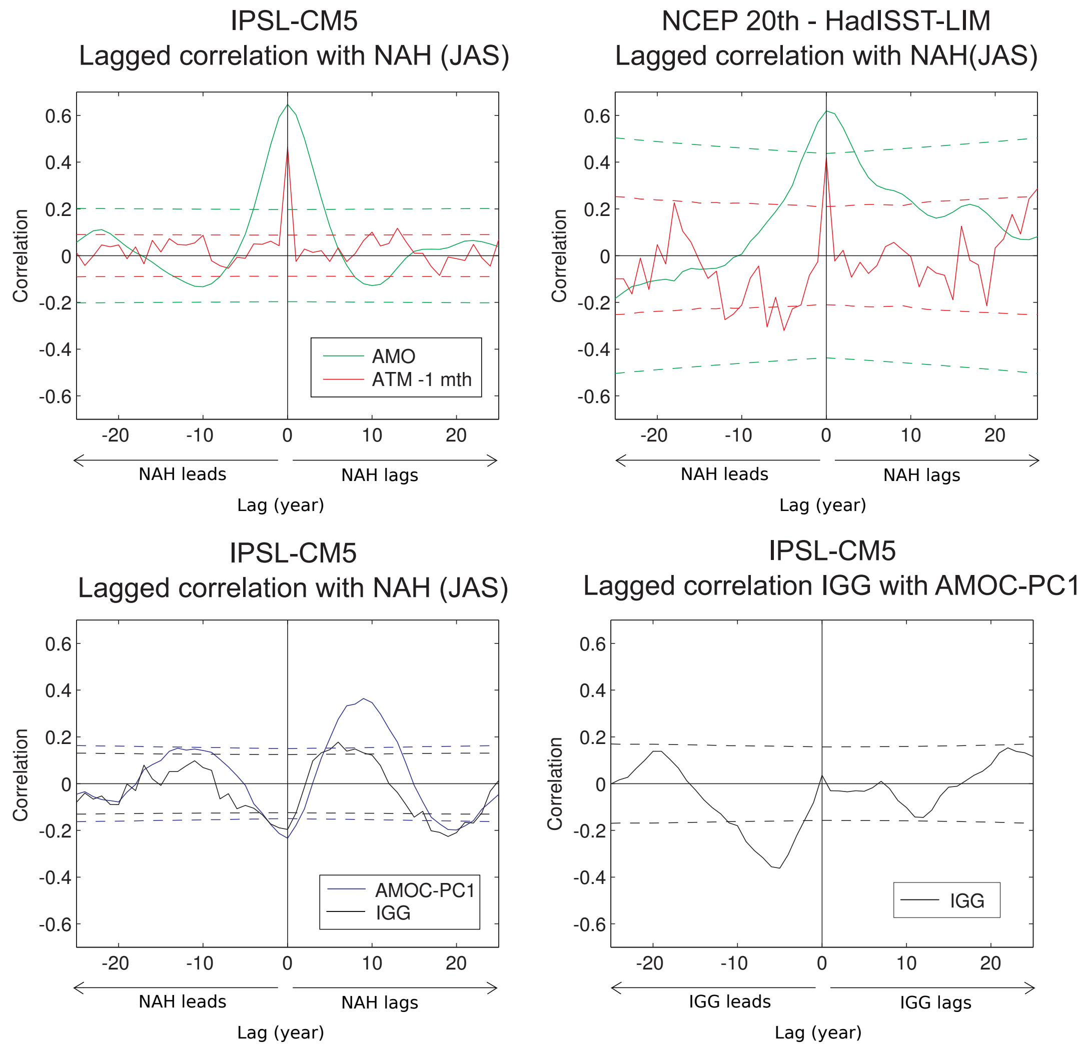

FIG. 13. (Upper panel) Temporal correlation between the NAH and the atmospheric forcing, and AMO in (left panel) IPSL-CM5 and (right panel) 20th century NCEP reanalysis and HadISST-LIM. (Lower-left panel) Temporal correlation between the NAH and the PC1 of the yearly AMOC (AMOC-PC1) and the intergyre gyre index (IGG) in IPSL-CM5. (Lower-right panel) Temporal correlation between the AMOC-PC1 and the intergyre gyre index (IGG) in IPSL-CM5. The lag is positive (negative) when the NAH lags (leads), except for lower-right panel where it is positive (negative) when the IGG lags (leads). The 5% significance of the correlation for each variable is given with dashed lines.

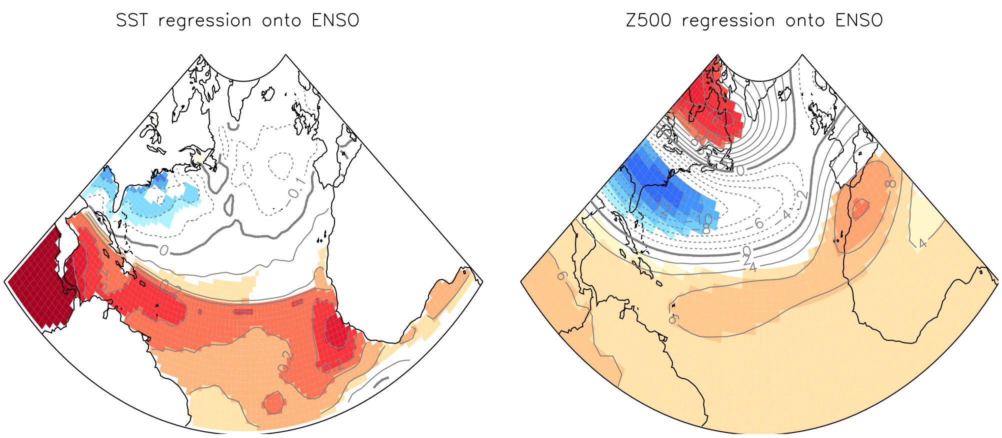

Fig. 14. Regression of the JFM (left panel) SST, in K, and (right panel) Z500, in m, onto the normalized ENSO index, in NCEP 20th century and HadISST-LIM. The ENSO index is the PC1 of the JFM SST in the Equatorial Pacific. The color shades are suppressed when the significance, given by Monte Carlo analysis, is above 5%.

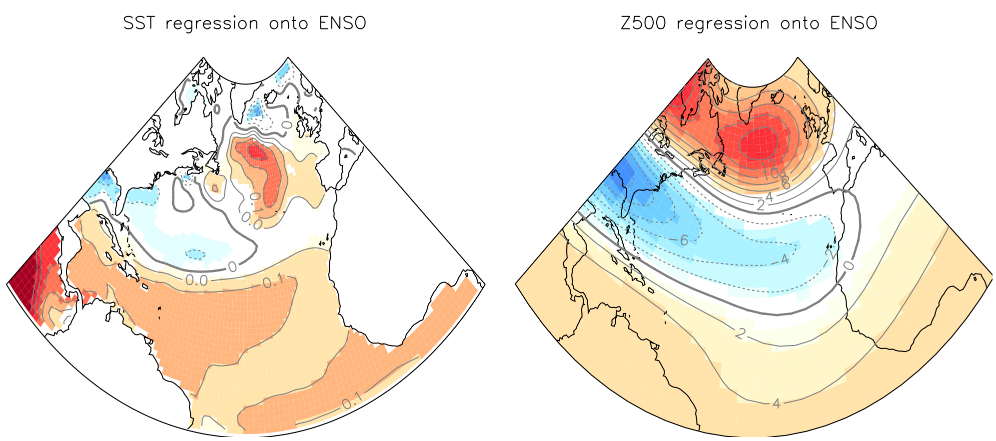

FIG. 15. Same as Fig. 14, but for IPSL-CM5 during JFM.